Structural definition of a pan-sarbecovirus neutralizing epitope on the spike S2 subunit.

Nicholas K. Hurlburt[1†], Leah J. Homad[1†], Irika Sinha[1], Madeleine F. Jennewein[1], Anna J. MacCamy[1], Yu-Hsin Wan[1], Jim Boonyaratanakornkit[1], Anton M. Sholukh[1], Panpan Zhou[2], Dennis R. Burton[2,3], Raiees Andrabi[2], Leonidas Stamatatos[1,4*], Marie Pancera[1*], Andrew T. McGuire[1,4,5*].

†Authors contributed equally

* Correspondence: amcguire@fredhutch.org; mpancera@fredhutch.org or lstamata@fredhutch.org

[1]Fred Hutchinson Cancer Research Center, Vaccine and Infectious Disease Division, Seattle, WA, USA

[2]Department of Immunology and Microbiology, The Scripps Research Institute, La Jolla, CA, USA

[3]Ragon Institute of MGH, MIT and Harvard, Cambridge, MA, USA

[4]Department of Global Health, University of Washington, Seattle, WA, USA

[5]Department of Laboratory Medicine and Pathology, University of Washington, Seattle, WA, USA

Abstract

Three highly pathogenic betacoronaviruses have crossed the species barrier and established human-to-human transmission causing significant morbidity and mortality in the past 20 years. The most current and widespread of these is SARS-CoV-2. The identification of CoVs with zoonotic potential in animal reservoirs suggests that additional outbreaks are likely to occur. Evidence suggests that neutralizing antibodies are important for protection against infection with CoVs. Monoclonal antibodies targeting conserved neutralizing epitopes on diverse CoVs can form the basis for prophylaxis and therapeutic treatments and enable the design of vaccines aimed at providing pan-coronavirus protection. To this end, we previously identified a neutralizing monoclonal antibody, CV3-25 that binds to the SARS-CoV-2 fusion machinery, neutralizes the SARS-CoV-2 Beta variant comparably to the ancestral Wuhan Hu-1 strain, cross neutralizes SARS-CoV-1 and displays cross reactive binding to recombinant proteins derived from the spike-ectodomains of HCoV-OC43 and HCoV-HKU1. Here, we show that the neutralizing activity of CV3-25 is also maintained against the Alpha, Delta and Gamma variants of concern as well as a SARS-CoV-like bat coronavirus with zoonotic potential by binding to a conserved linear peptide in the stem-helix region on sarbecovirus spikes. A 1.74Å crystal structure of a CV3-25/peptide complex demonstrates that CV3-25 binds to the base of the stem helix at the HR2 boundary to an epitope that is distinct from other stem-helix directed neutralizing mAbs. Thus, CV3-25 defines a novel site of sarbecovirus vulnerability that will inform pan-CoV vaccine development.

Introduction

Coronaviruses (CoVs) are a large family of viruses that infect many species of birds and mammals, including humans. They are subdivided into four genera; alpha, beta, gamma and delta. Two alpha CoVs, NL63 and 229E, and two beta CoVs (OC43 and HKU1) are endemic in the human population and cause mild respiratory cold like symptoms (Cui et al., 2019). Three separate zoonotic transmissions of highly pathogenic beta CoVs to humans have been documented in the last two decades.

Middle East respiratory syndrome coronavirus (MERS-CoV) first emerged in Saudi Arabia in 2012 and has since been detected in 27 countries (Zaki et al., 2012). There have been ~2,574 reported MERS cases resulting in 884 deaths (35.4% mortality rate). Most cases of MERS are attributed to zoonotic transmission from camels causing clusters of human-to-human transmission among subjects who have close contact, usually in health care settings (Killerby et al., 2020).

SARS-CoV-1 was first identified as the causative agent of atypical respiratory syndrome called Severe Acute Respiratory Syndrome in China in 2002. SARS-CoV-1 subsequently spread to 29 countries and infected 8098 people causing 774 deaths (9.5% mortality rate). More recently, the highly transmissible SARS-CoV-2 virus emerged in China and rapidly spread through the global population. SARS-CoV-2 has infected ~185 million people and caused over 4 million deaths (Dong et al., 2020). SARS-CoV-2 and SARS-CoV-1 are members of the sarbecovirus subgenus and share ~80% amino acid sequence identity (Wan et al., 2020). SARS-CoV-2 is highly similar to a bat CoV, RaTG13 (Zhou et al., 2020). Several other SARS-like bat coronaviruses

have been identified that have zoonotic potential (Cui et al., 2019) suggesting that both viruses likely originated in bats.

CoV infection is mediated by the viral spike protein (S) which is a membrane anchored class I fusion protein expressed on the virion surface and is an important target of host immune responses elicited by infection or vaccination. S is comprised of two distinct functional subunits; a N-terminal, membrane distal subunit designated S1 and a C-terminal, membrane proximal subunit designated S2. The S2 domain houses the fusion machinery that undergoes large structural rearrangements to mediate fusion of the host and viral membranes. The S1 domain serves to stabilize the S2 subunit in the pre-fusion state and facilitates the attachment to ligands on host cells through the receptor binding domain (RBD)(Tortorici and Veesler, 2019). Cell fusion requires conformational changes induced by receptor binding, as well as further proteolytic cleavage of the S2 subunit to liberate the fusion peptide and trigger conformational changes, which can occur at the cell membrane or following viral endocytosis (Millet and Whittaker, 2015).

Despite the overall structural similarity of their S proteins, human coronaviruses use diverse entry receptors (Tortorici and Veesler, 2019, Walls et al., 2020, Wrapp et al., 2020). 229E uses human aminopeptidase N (hAPN), while HKU1 and OC43 cell-entry depends on 9-O-acetylated sialic acids (Vlasak et al., 1988, Tortorici and Veesler, 2019, Yeager et al., 1992). NL63, SARS-CoV-1 and SARS-CoV-2 use angiotensin converting enzyme 2 (ACE2) (Hoffmann et al., 2020, Li et al., 2003, Walls et al., 2020, Hofmann et al., 2005). SARS-CoV-2 also uses heparan sulfate as an attachment factor to promote infection (Clausen et al., 2020). MERS-CoV utilizes sialoside receptors as

attachment factors and dipeptidyl peptidase 4 (DPP4) as an entry receptor (Park et al., 2019, Raj et al., 2013).

Due to extensive CoV genetic diversity, wide range of animal hosts, and potential for zoonotic transmission there is a need for vaccines and therapeutic agents that can prevent or limit future outbreaks (Ghai et al., 2021, Woo et al., 2009). Neutralizing antibodies elicited by vaccination or natural infection are an important correlate of protection against subsequent CoV infection (McMahan et al., 2020, Khoury et al., 2021, Lumley et al., 2021). Further, passive delivery of monoclonal neutralizing antibodies can be used as a countermeasure to prevent CoV-related illness (Weinreich et al., 2021).

The primary targets of neutralizing antibodies are within the S1 subunit: the receptor binding domain (RBD) and the N-terminal domain (NTD) (McCallum et al., 2021, Piccoli et al., 2020, Stamatatos et al., 2021, Cerutti et al., 2021, Brouwer et al., 2020, Rogers et al., 2020, Cao et al., 2010, Rockx et al., 2008, Hwang et al., 2006, Prabakaran et al., 2006, Sui et al., 2004, Traggiai et al., 2004, Ying et al., 2014, Tang et al., 2014, Jiang et al., 2014, Niu et al., 2018, Eguia et al., 2020, Kistler and Bedford, 2021, Liu et al., 2020, Chi et al., 2020). Due to the diversity in receptor usage and variability of spike sequences across CoVs, RBD and NTD directed mAbs are often virus specific. Even within the same CoV, mutant variants can evade neutralization by monoclonal antibodies (mAbs) and polyclonal sera. Indeed, mutations found in the RBD and NTD of SARS-CoV-2 variants of concern are responsible for increased resistance to serum and monoclonal antibodies. It has been speculated such variants could erode vaccine efficacy over time. The RBD and NTD of other CoVs appear to be subject to

and evade immune pressure as well (Kistler and Bedford, 2021, Eguia et al., 2020). In contrast, S2 is more functionally and structurally conserved among CoVs (Tortorici and Veesler, 2019, Shah et al., 2021). However, it is sub-dominant with respect to neutralizing antibody responses as the majority of S2-binding mAbs isolated from SARS-CoV-2 infected donors are non-neutralizing (Rogers et al., 2020, Brouwer et al., 2020, Sakharkar et al., 2021, Jennewein et al., 2021, Andreano et al., 2021).

We recently described the isolation of a neutralizing anti-S2 mAb, CV3-25 from a SARS-CoV-2 infected donor (Jennewein et al., 2021). The neutralizing potency of CV3-25 is unaffected by mutations found in the Beta (B.1.351) SARS-CoV-2 variant and can neutralize SARS-CoV-1. CV3-25 also displays cross-reactivity with recombinant spike proteins derived from the betaCoVs, OC43 and HKU1. Here, we demonstrate that the neutralizing activity of CV3-25 is unaffected by mutations found in the Alpha, Delta and Gamma variants and show that it can neutralize a SARS-like bat CoV, WIV1 (Ge et al., 2013). We identified a linear epitope overlapping the stem-helix/HR2 region containing the epitope of CV3-25. A crystal structure of CV3-25 with a 19mer peptide revealed that CV3-25 binds to a solvent-exposed linear epitope that partially unwinds the stem-helix. The CV3-25 epitope is distinct from other mAbs targeting the stem helix region (Sauer et al., 2021, Pinto et al., 2021, Zhou et al., 2021), thus defining a novel site of conserved vulnerability that will enable pan-CoV vaccine design.

Results

CV3-25 neutralizes SARS-CoV-2 variants and a SARS-like bat coronavirus.

We previously reported that CV3-25 neutralizes the Wuhan-Hu-1 and Beta (B.1.351) variants of SARS-CoV-2 with comparable potency (Jennewein et al., 2021). Here we evaluated the ability of CV3-25 to neutralize additional SARS-CoV-2 variants Alpha (B.1.1.7), Delta (B.1.617.2) and Gamma (P.1) and a more distantly related SARS-like bat coronavirus, WIV1, which uses ACE2 as an entry receptor and can infect human cell lines. (Ge et al., 2013, Rambaut et al., 2020, Tegally et al., 2020, Faria et al., 2021). Therefore, W1V1 represents a bat CoV with pandemic potential. CV3-25 neutralized all variants and WIV1 with comparable potency (Fig. 1A). In contrast, the RBD-directed CV30 mAb showed reduced potency against the Beta and Gamma variants of concern, both of which harbor mutations in the RBD at position 417 that makes direct contact with CV30 (Hurlburt et al., 2020, Faria et al., 2021, Tegally et al., 2020) (Fig. 1B). WIV1 was completely resistant to CV30-mediated neutralization. Combined with the observation that CV3-25 also neutralizes SARS-CoV-1, these data indicate that it binds to an epitope on S2 that is unaffected by mutations found in these variants.

CV3-25 binds to a linear epitope on the SARS-CoV-2 stem helix.

A handful of S2-directed neutralizing mAbs that display varying degrees of CoV cross-binding and/or neutralizing activity have been isolated. A semi-conserved site of vulnerability defined by the 3A3 mAb maps to the membrane-distal end of the pre-fusion S2 subunit and several mAbs have been found to bind the stem helix at the base of the S2 spike (Huang et al., 2021, Wang et al., 2021, Pinto et al., 2021, Zhou et al., 2021, Song et al., 2020). Based on the ability of CV3-25 to neutralize diverse sarbecovirueses (Fig. 1) and the fact that it can bind the ectodomains from additional betacoronaviruses

157 SARS-CoV-1, OC43, and HKU1 (Jennewein et al., 2021), we hypothesized that CV3-25
158 was binding to one of these semi-conserved regions. To test this, we evaluated the
159 ability of the stem helix-directed mAb B6 (Sauer et al., 2021) to bind to the recombinant
160 SARS-CoV-2 spike in the presence of CV3-25. B6 neutralizes pseudoviruses
161 expressing the spike proteins from MERS-CoV, HCoV-OC43 and the MERS-like bat
162 CoV HKU4. It binds to but does not neutralize SARS-CoV-1 and SARS-CoV-2 (Sauer et
163 al., 2021). B6 readily bound to the S2P protein as measured by biolayer interferometry
164 (BLI) but was unable to bind to an S2P-CV3-25 complex indicating that the antibodies
165 compete for binding to the SARS-CoV-2 spike (Fig. 2A).

166 B6 binds to a linear peptide spanning amino acids 1147-1157 of the SARS-CoV-
167 1/SARS-CoV-2 stem helix (Sauer et al., 2021). To test whether CV3-25 binds to a
168 similar epitope, CV3-25 binding to overlapping 15mer linear peptides spanning the stem
169 helix region (1143-1162) from SARS-CoV-2 was measured by ELISA (Fig. 2B-C). CV3-
170 25 bound to two peptides encompassing amino acids 1149-1163 and 1153-1167, with
171 stronger binding to the latter (Fig. 2C). CV3-25 did not bind to any of the other SARS-
172 CoV-2 peptides or to a control peptide from HIV-1 Env. CV3-25 binding was specific, as
173 CV2-10, an S2 directed mAb that does not compete with CV3-25 binding (Jennewein et
174 al., 2021), did not bind either peptide. To confirm binding to this peptide region, we
175 synthesized a peptide spanning 1145-1167 and verified that CV3-25 bound to the
176 peptide with ~5nM affinity using biolayer interferometry (BLI). The measured affinity of
177 CV3-25 for the peptide is lower than it is for a recombinant stabilized spike protein (~0.6
178 nM) (Fig. 2F and Table S2). We note that the association rate of binding to the peptide
179 does not fit well to a 1:1 binding model (Fig. 2E) which may reflect several

conformations sampled by the immobilized peptide (a heterogenous ligand) and affect the accuracy of the CV3-25 peptide binding measurement.

Structure of CV3-25 reveals a novel site of vulnerability in S2

To gain insight into the nature of the CV3-25 peptide interaction, the antigen binding fragment (Fab) of CV3-25 was complexed with a synthesized peptide of the C-terminal end of the stem helix (residues 1149-1167). A crystal structure of the Fab-peptide complex was obtained to a resolution of 1.74 Å (Supplementary Table 1). The structure showed that binding to this peptide is almost entirely heavy chain dependent (Fig. 3A and B). The N-terminal end of the peptide forms an α-helix that is engaged by the CDRH1 and CDRH2. The CDRH3 extends under the base of the α-helix directing the extended C-terminal portion of the peptide up into the CDRH1 before turning downward to interact with the light chain. The Fab binds the peptide with a total buried surface area (BSA) of ~594 $Å^2$, of which ~516 $Å^2$ is from the heavy chain and ~78 $Å^2$ from the light chain (Fig. 3C).

Alanine scanning of a stem helix peptide was conducted to assess the relative contributions of the interactions observed in the crystal structure (Fig. 3D). This analysis revealed that mutating Lys_{1157}, any of the residues in $_{1160}TSPDV_{1164}$, or Leu_{1166} inhibited or greatly reduced binding (Fig. 3D). This data agrees well with the structural data. Lys_{1157} buries ~133 $Å^2$ upon binding, the highest amount of BSA on the peptide, and forms hydrogen bonds with two Asp residues in the CDRH2 (Fig. 3E). $_{1160}TSPDV_{1164}$ is the segment of peptide just after the helix that interacts with CDRH3 before curving up to interact with CDRH1 and then the light chain.

Reversion of CV3-25 to the inferred germline (iGL) version abrogated CV3-25 neutralizing activity despite showing comparable binding to SARS-CoV-S2P under avid conditions (Jennewein et al., 2021). Although the majority of the mAb-peptide contacts are through the CDRH3, Arg_{31} in the CDRH1 buries the most surface area (75 $Å^2$) in the CV3-25-peptide structure (Fig. 3C). Arg_{31} forms a water-mediated interaction with Asp_{1153} and a π-stacking interaction with Phe_{1156} on the peptide. The germline encoded Ser at the position would be incapable of forming these interactions providing a rationale for the lack of neutralizing activity of iGL-CV3-25.

Structural alignment of the stem helix peptides in the CV3-25 and B6 structures show that CV3-25 binds more C-terminal than B6 in the stem helix (Fig. 4A) in agreement with the binding to overlapping linear peptides (Fig.2C). The stem helix residues that are shared in the structures adopt almost identical conformations (Fig. 4A). B6 binds to the hydrophobic face of the amphipathic helix that is predicted to be on the interior of the stem helix bundle of the pre-fusion trimer (Sauer et al., 2021). In contrast, CV3-25 binds to the solvent-exposed hydrophilic face of the helix. An alignment of the CV3-25 stem helix to a cryoEM structure of the native prefusion spike with the stem helix structure resolved (PDBID: 6XR8)(Cai et al., 2020) indicates that the CV3-25-bound stem helix unwinds a full turn, with the helix terminating Pro_{1162} moving ~13Å into the interior of the helix bundle (Fig. 4B). The unwinding and repositioning of the stem-helix by CV3-25 would create a clash between residues $_{1162}$PDVDL$_{1166}$ and the CDRH1 and CDRH3 of B6. There are additional potential clashes between the CDRH3 on CV3-25 and CDRH2 on B6. Collectively these provide a structural basis for the observed competition between B6 and CV3-25 binding to SARS-CoV-2 S2P, which was

confirmed using a linear SARS-CoV-2 peptide (Fig. S2). CV3-25 binding to the stem helix peptide also prevented subsequent binding of the CC40.8 mAb (Fig. S2), which binds to an epitope that is nearly identical to B6 and weakly neutralizes SARS-CoV-1 and SARS-CoV-2 (Zhou et al., 2021, Song et al., 2020). CryoET analysis of the SARS-CoV-2 spike on the surface of intact virions shows an extended stalk region downstream of the stem helix (Turonova et al., 2020, Ke et al., 2020). However, all presently available CryoEM structures of the stabilized or membrane solubilized native spikes show poor resolution of the stem helix region and density for the downstream region including HR2 is missing (Walls et al., 2020, Wrapp et al., 2020, Cai et al., 2020). A model of the full length spike ectodomain, including HR2 was determined using homology modelling and molecular dynamic (MD) simulation (Casalino et al., 2020). Aligning the CV3-25-stem helix structure to this model shows good agreement (Fig. 4C). In both the modeled and CV3-25-peptide structures, the stem helix ends at the glycosylated Asn_{1158}, and the extended C-terminal end of the CV3-25 bound peptide adopts a similar conformation to the MD model.

The linear peptide in the CV3-25 structure contains one putative N-linked glycosylation site at Asn_{1158}. This glycan is not predicted to clash with CV3-25 binding to the peptide, but in the 6XR8 trimer with the extended stem helix, the glycan on one of the adjacent protomers would potentially clash with the heavy chain of the antibody (Fig. 4B). In the MD model, the glycan on the adjacent protomer shifts so that it is no longer clashing with the heavy chain (Fig. 4C). Additionally, the alignment of the model also suggests that the light chain of CV3-25 could potentially bind to the region just

downstream of the stem helix at the start of HR2, $_{1168}$DISGINASVVN$_{1178}$ (Fig. 4D), a region that shows some sequence conservation amongst coronaviruses (Fig. 4E).

Superimposition of the CV3-25/peptide structure onto the post-fusion structure of SARS-CoV-2 spike (PDBid: 6XRA) reveals a different conformation of the CV3-25 epitope (Fig. 4F) (Cai et al., 2020). In the post-fusion conformation, the stem helix in this epitope unwinds a full turn, relative to the CV3-25 bound peptide, with the remainder of the stem-helix elongating into a more linear structure. The overall RMSD between the CV3-25 bound peptide and this region in the post-fusion spike is 9.757 Å^2 over 15 Cα atoms and is therefore unlikely to be compatible with CV3-25 binding. Thus, CV3-25 may prevent the transition of the SARS-CoV-2 spike from the pre-fusion to the post-fusion form. In line with this notion, CV3-25 inhibits spike mediated syncytia formation in vitro (Ullah et al., 2021).

Cross-reactivity of CV3-25 with the stem helix of other CoVs

Several of the CV3-25 contact residues are conserved in beta CoVs (Fig. 4E). We therefore evaluated the ability of CV3-25 to bind peptides derived from additional Beta-CoVs spanning the stem helix region by ELISA. CV3-25 bound equally well to peptides derived from SARS-CoV-1/2/WIV1, MERS-CoV, and HCoV-OC43. CV3-25 binding was slightly weaker to a peptide derived from HCoV-HKU1 (Fig. 5A), consistent with HKU1 having fewer conserved contact residues (Fig. 4E). Qualitative binding to SARS-CoV-1/2/WIV1, MERS-CoV, HCoV-OC43 and HCoV-HKU1 was confirmed by BLI (Fig. S3). This analysis also revealed a lack of binding to corresponding peptides from the alpha CoVs HCoV-229E and HCoV-NL63 (Fig. S3), consistent with a lack of

CV3-25 binding to recombinant HCoV-229E and HCoV-NL63 spike proteins (Jennewein et al., 2021).

In contrast, the stem-helix directed mAbs B6 and CC40.8 showed differential binding to these peptides. B6 bound most strongly to the peptide from MERS-CoV, followed by HCoV-OC43, SARS-CoV-2 and HCoV-HKU1 (Fig. 5B), while CC40.8 exhibited the strongest binding to HCoV-HKU1, followed by MERS and HCoV-OC43 (Fig. 5C). We were unable to detect binding of CC40.8 to the SARS-CoV-2 peptide at the concentration tested here. To assess whether CV3-25 could bind to the linear epitope presented on these peptides in the context of a full-length spike protein, we expressed the membrane anchored, wildtype spike proteins from SARS-CoV-2, SARS-CoV-1, WIV1, HCoV-OC43, HCoV-HKU1, and MERS-CoV on the surface of 293 cells and stained them with fluorescently labeled CV3-25. We included B6, CC40.8, CV30 and AMMO1 mAbs for comparison. CV3-25 bound to SARS-CoV-2, SARS-CoV-1, WIV1, consistent with its ability to bind to the stem helix peptide from these spike proteins and neutralize the corresponding pseudoviruses (Fig. 5E-G). Despite binding to the stem helix peptide from MERS-CoV, HCoV-OC43 and HCoV-HKU1, and stabilized soluble versions of the corresponding spike ectodomains (Fig. S4), CV3-25 did not recognize cell-surface expressed spikes (Fig. 5H-J). In line with the lack of binding, CV3-25 failed to neutralize a MERS-CoV pseudovirus or authentic HCoV-OC43 (Fig. 5K and M). Similarly, a monovalent Fab was unable to neutralize HCoV-OC43, indicating that the lack of neutralization was not due to steric shielding of the epitope from full length IgG (Fig. 5L). CV3-25 was also unable to neutralize authentic HCoV-NL63, an alpha CoV (Fig. S5). We conclude that although the CV3-25 epitope is present, it is not

292 equally accessible in the native conformation of the spike protein among the various
293 beta CoVs examined here.

294 **Somatic mutation leads to stronger cross-reactive binding by CV3-25**

295 To assess the role of somatic mutation in CV3-25 cross-reactivity we measured
296 the binding of iGL-CV3-25 to the same linear peptides from SARS-CoV-2, MERS-CoV,
297 HCoV-OC43 and HCoV-HKU1 by ELISA (Fig. 5D). Although the binding to the peptide
298 from SARS-CoV-1/2 and WIV1 was comparable and strong, the binding was severely
299 reduced to MERS and OC43, and to a lesser extent to HKU1. Thus, somatic mutations
300 acquired by CV3-25 lead to broad CoV-peptide reactivity.

301

Discussion

The devastating loss of life, economic and social impacts of the SARS-CoV-2 pandemic underscores the need to prevent future CoV outbreaks. The fact that SARS-CoV-2 is the third highly pathogenic CoV to cause significant loss of human life in the past two decades suggests that future CoV outbreaks are plausible if not inevitable. Since neutralizing antibodies are likely important for protection against CoV infection, the isolation and characterization of mAbs targeting conserved neutralizing epitopes present across CoV variants and strains can inform the design of pan-CoV vaccines that can prevent or blunt future outbreaks.

So far, six neutralizing mAbs targeting the stem-helix region, elicited by immunization in mice, or humanized mice (B6, 1.6C7 and 28D9), or isolated from SARS-CoV-2 infected humans (CC40.8, S2P6, CV3-25), have been described (Sauer et al., 2021, Wang et al., 2020, Zhou et al., 2021, Pinto et al., 2021, Jennewein et al., 2021). All show varying degrees of cross-reactivity and cross-neutralizing activity against CoVs. Among these mAbs, three S2P6, CC40.8 and B6 have previously been structurally characterized. All form a hydrophobic groove that cradles the hydrophobic face of the amphipathic SARS-CoV-2 stem helix (residues AA 1147-1156 for B6, residues 1142-1159 for CC40.8 and residues 1146-1159 for S2P6). Alanine scanning of a stem helix peptide from MERS S suggests that the 1.6C7 and 28D9 mAbs which were isolated from humanized mice immunized sequentially with recombinant S from OC43, SARS and MERS, bind to a similar epitope region (Wang et al., 2021). In contrast to the other stem helix mAbs, CV3-25 binds to a distinct S2 epitope C terminal and on the

opposite face of the amphipathic stem helix thus defining an additional site of vulnerability on pathogenic beta CoVs.

Very little high-resolution structural information is available about the conformation of the stem helix, and region C-terminal to the stem-helix. As such, we can only speculate as to why CV3-25 binds well to recombinant spike ectodomains and linear peptides from the MERS-CoV, HCoV-OC43 and HCoV-HKU1 Beta CoVs, but fails to bind full-length cell-surface expressed spikes or neutralize the corresponding viruses/pseudoviruses. CryoEM structures of stabilized NL63, MERS-CoV, SARS-CoV, and SARS-CoV-2 spike proteins only resolve the N-terminus of the stem-helix region (Walls et al., 2020, Walls et al., 2019, Wrapp et al., 2020, Kirchdoerfer et al., 2018, Yuan et al., 2017, Gui et al., 2017, Pallesen et al., 2017). Moreover, complexes of mAbs B6, S26P and CC40.8 with stabilized spikes from MERS, SARS-CoV-2 and HKU1 are also poorly resolved by EM suggesting that this region undergoes significant conformational heterogeneity on recombinant proteins (Song et al., 2020, Sauer et al., 2021, Pinto et al., 2021). Subtomogram averaging of virion-anchored SARS-CoV-2 spikes show evidence of flexible hinges in the stalk region (Ke et al., 2020, Turonova et al., 2020). The stalk has been likened to a leg with a hip, knee and ankle joint where the stem helix region corresponds to the upper leg (Turonova et al., 2020). CV3-25 would bind to the dynamic “knee” region and may only recognize one of many conformations adopted by the SARS-CoV-2 spike. If so, it’s possible that a similar conformation is not sampled by membrane-anchored MERS, HKU1 or OC43 spikes.

Alternatively, the CV3-25 epitope could be less exposed in the context of the MERS, OC43 and HKU1 membrane-anchored spikes as compared to their

corresponding stabilized ectodomains or the membrane-anchored sarbecovirus spikes. We note however, that the smaller size Fab domain of CV3-25 was unable to neutralize the OC43 virus.

It has been proposed that the B-cell lineages that gave rise to the stem helix mAbs CC40.8 and S26P were initiated by previous OC43 and HKU1 infection, respectively (Song et al., 2020, Pinto et al., 2021). Despite binding to linear peptides from HKU1 and to a lesser extent OC43, the absence of CV3-25 reactivity with membrane-anchored spikes from endemic HCoVs suggests that the CV3-25 progenitor B cell was activated by the SARS-CoV-2 virus rather than a prior HCoV-infection.

The neutralizing potency of CV3-25 is not affected by mutations found in SARS-CoV-2 variants of concern, which harbor mutations that escape from many anti-NTD and anti-RBD antibodies. Moreover, the CV3-25 epitope is strictly conserved among SARS-CoV-1, SARS-CoV-2 and WIV1; the antibody neutralizes pseudoviruses expressing all three spikes, and displays anti-viral activity in K18-hACE2 mice, particularly when Fc receptors are engaged (Ullah et al., 2021).

We propose that the CV3-25 epitope is highly relevant to the development of a pan-sarbecovirus vaccine. The fact that CV3-25 binds a linear epitope indicates that it may be possible to design small scaffold based, or subunit vaccines that present the CV3-25 epitope while avoiding eliciting an immunodominant response to non-neutralizing epitopes on S2 and elsewhere on the spike. The observation that CV3-25 competes for binding with B6 and CC40.8 despite binding to discrete linear epitopes, indicates that multiple scaffold design strategies may need to be employed to target these two conserved sites of CoV vulnerability in the stem-helix region in order to

370 provide broad neutralizing coverage against diverse CoV. Similarly, a therapeutic
371 combination of non-competing stem-helix mAbs may provide broad neutralizing
372 coverage against emergent pathogenic CoVs since CV3-25 neutralizes diverse
373 sarbecoviruses, and B6 neutralizes multiple merbecoviruses and OC43, a member of
374 the embecovirus subgenus (Sauer et al., 2021)

375

Material and Methods

Cell Lines

All cell lines were incubated at 37°C in the presence of 5% CO2. 293-6E (human female, RRID:CVCL_HF20) and 293T cells (human female, RRID:CVCL_0063) cells were maintained in Freestyle 293 media with gentle shaking. HEK-293T-hACE2 (human female, BEI Resources Cat# NR-52511) were maintained in DMEM containing 10% FBS, 2 mM L-glutamine, 100 U/ml penicillin, and 100 µg/ml streptomycin (cDMEM). HCT-8 [HRT-18] cells (human male, ATCC CCL-244) were maintained in RPMI containing 10% horse serum, 2 mM L-glutamine, 100 U/ml penicillin, and 100 µg/ml streptomycin. LLC-MK2 cells (*Macaca mulatta,* ATCC CCL-7) were maintained in cDMEM. Huh7 cells (human male, a gift from Dr. Ram Savan, Department of Immunology University of Washington) were maintained in cDMEM.

Recombinant CoV proteins and mAbs

Two stabilized versions of the recombinant SARS-CoV-2 spike protein (S2P and S6P) and the SARS-CoV-2 RBD were produced in 293E cells and purified as previously described (Seydoux et al., 2020, Jennewein et al., 2021). Plasmids encoding the stabilized versions of HCoV-OC43 (619-M66-303: CMV51p> HCoV-OC43 S-2P-T4f-3C-His8-Strep2x2, Addgene plasmid # 166015) and HCoV-HKU1 (R619-M89-303: CMV51p> HCoV-HKU1 S-2P-T4f-3C-His8-Strep2x2, Addgene plasmid # 166014) were gifts from Domonic Esposito. The proteins were expressed in 293E cells and purified using Ni-NTA affinity resin followed by size exclusion chromatography on a superose 6

column as described in(Esposito et al., 2020). Recombinant CV3-25, CV30, B6 and AMMO1 were expressed in 293 cells and purified using protein A resin as previously described (Sauer et al., 2021, Jennewein et al., 2021, Snijder et al., 2018).

Generation of plasmids expressing SARS-CoV-2 spike variants and MERS-CoV.

To generate a plasmid encoding the SARS-CoV-2 spike P.1 variant (pHDM-SARS-CoV-2-Spike-P.1) primers were designed that anneal 5' of the L18 codon and just 3' of the V1176F codon on the pHDM-SARS-CoV-2 Spike Wuhan-Hu-1 plasmid (BEI Resources Cat# NR-52514) and used to amplify cDNA corresponding to the N and C termini of the spike protein and the plasmid backbone using Platinum SuperFi II DNA Polymerase (Thermofisher Cat# 12368010) according to the manufacturer's instructions. cDNA encoding the rest of the spike protein including the Δ242-243 deletion and the L18F, T20N, P26S, D138Y, R190S, K417T, E484K, N501Y, D614G, H655Y, T1027I, and V1176F mutations was synthesized as two gBlocks (Integrated DNA technologies). The first had 30nt of homology with the PCR amplified vector backbone at the 5' end. The second included 30nt of homology with the 3' end of the first block at the 5' end and 30nt of homology with the PCR amplified vector backbone at the 3' end. The gBlocks and PCR product were ligated together using InFusion HD cloning Plus (TakaraBio Cat#638920). To generate a plasmid encoding the SARS-CoV-2 spike B.1.1. variant (pHDM-SARS-CoV-2-Spike-B.1.1.7) primers were designed that anneal 5' of the H69 codon and just 3' of the D1118 codon on the pHDM-SARS-CoV-2 Spike Wuhan-Hu-1 plasmid (BEI Resources Cat# NR-52514) and used to amplify cDNA corresponding to the N and C termini of the spike protein and the plasmid backbone using Platinum SuperFi II DNA Polymerase (Thermofisher Cat# 12368010) according to the

manufacturer's instructions. cDNA encoding the rest of the spike protein including the H69-V70 and Y144 deletions, N501Y, A570D, D614G, P681H, T716I, S982A and D1118H mutations. A plasmid encoding the SARS-CoV-2 Spike B.1.617.2 (pCMV3-SARS-CoV-2-Spike-B.1.617.2) was purchased from Sinobiological (Cat# VG40804-UT).

To generate a plasmid encoding the MERS-CoV-2 spike (pHDM-MERS-CoV-Spike) codon-optimized cDNA corresponding to the MERS-CoV S protein (Riyadh_14_2013, GenBank: AHI48572.1) flanked on the 5' end by 30nt of homology upstream of and including the EcoRI site and flanked on the 3' end by 30nt of homology downstream of and including the HindIII site on the pHDM-SARS-CoV-2 Spike Wuhan-Hu-1 plasmid was synthesized by Twist Biosciences. The synthesized DNA was cloned into the pHDM-SARS-CoV-2 Spike Wuhan-Hu-1 plasmid that was cut with EcoRI and HindIII and gel purified to remove the SARS-CoV-2 Spike cDNA using InFusion HD cloning Plus. The sequences of the cDNA of all the spike expression constructs were verified by Sanger sequencing (Genewiz Inc.).

Peptides

Peptides were synthesized by Genscript or A&A Labs with, or without a biotin molecule conjugated to the amino-terminus via aminohexanoic acid.

Pseudovirus neutralization assay

HIV-1 derived viral particles were pseudotyped with full length wildtype S from Wuhan Hu1, B.1.351, B.1.1.7, P.1, WIV1, or MERS-CoV using a previously described reporter system (Crawford et al., 2020). Briefly, plasmids expressing the HIV-1 Gag and pol (pHDM540 Hgpm2, BEI Resources Cat# NR-52517), HIV-1Rev (pRC-CMV-rev1b, BEI

Resources Cat# NR-52519), HIV-1 Tat (pHDM-tat1b, BEI resources NR-52518), SARS-CoV-2 spike (pHDM-SARS-CoV-2 Spike Wuhan-Hu-1, pHDM-SARS-CoV-2 Spike-B.1.1.7, SARS-CoV-2 Spike-P.1, pHDM-SARS-CoV-2 Spike-B.1.351 (Stamatatos et al., 2021), pCMV3-SARS-CoV-2-Spike-B.1.617.2, pTWist-WIV1-CoV (a gift from Alejandro Balazs (Addgene plasmid # 164438 ; http://n2t.net/addgene:164438 ; RRID:Addgene_164438), or pHDM-MERS-CoV Spike and a luciferase/GFP reporter (pHAGE-CMV-Luc2-IRES542 ZsGreen-W, BEI Resources Cat# NR-52516) were co-transfected into 293T cells at a 1:1:1:1.6:4.6 ratio using 293 Free transfection reagent according to the manufacturer's instructions. Pseudoviruses lacking a spike protein were also produced as a control for specific viral entry. Pseudoviron production was carried out at 32 ˚C for 72 hours after which the culture supernatant was harvested, clarified by centrifugation and frozen at -80˚C.

293 cells stably expressing human HEK-293T-hACE2, for SARS-CoV-2 pseudoviruses, or Huh-7 cells for MERS-CoV pseudoviruses were seeded at a density of $4x10^3$ cells/well in a 100 µL volume in 96-well flat bottom black-walled, clear bottom tissue culture plates (Greiner CELLSTAR Cat# 655090). The next day, mAbs were serially diluted in 70 µL of cDMEM in 96-well round bottom master plates in duplicate wells. 30 µL of serially diluted mAbs from the master plate were replica plated into 96-well round bottom plates. An equal volume of viral supernatant was added to 96-well round bottom plates containing identical serial dilutions from the same master plate, and incubated for 60 min at 37 ˚C. Meanwhile 50 µL of cDMEM containing 6 µg/mL polybrene was added to each well of 293T-ACE2 or Huh-7 target cells and incubated for 30 min. The media was aspirated from target cells and 100 µL of the virus-antibody mixture was added.

The plates were incubated at 37˚C for 72 hours. The supernatant was aspirated and replaced with 100 µL of Steady-Glo luciferase reagent (Promega Cat# E2510) and read on a Fluoroskan Ascent Fluorimeter. Control wells containing virus but no antibody (cells + virus) and no virus or antibody (cells only) were included on each plate.

Percent neutralization for each well was calculated as the RLU of the average of the cells + virus wells, minus test wells (cells + mAb + virus), and dividing this result difference by the average RLU between virus control (cells + virus) and average RLU between wells containing cells alone, multiplied by 100. The antibody concentration that neutralized 50% or 80% of infectivity (IC50 and IC80 for mAbs) was interpolated from the neutralization curves determined using the log(inhibitor) vs. response -- Variable slope (four parameters) fit using automatic outlier detection in GraphPad Prism Software.

Biolayer interferometry (BLI)

BLI experiments were performed on an Octet Red instrument at 30°C with shaking at 500-1000 rpm.

Kinetics analysis:

Streptavidin (SA) biosensors (Fortebio) were immersed Kinetics Buffer (KB: 1X PBS, 0.01% Tween 20, 0.01% BSA, and 0.005% NaN3, pH 7.4) containing 10µg/ml of biotinylated peptides for 150s, followed by immersion in KB for 60s to achieve a baseline reading. Probes were then immersed in KB containing serially diluted CV3-25 Fab for a 300s association phase, followed by a 300s dissociation phase in KB. The background signal from each analyte-containing well was measured using empty

reference sensors and subtracted from the signal obtained with each corresponding mAb loaded sensor. Kinetic analyses were performed at least twice with an independently prepared analyte dilution series. Curve fitting was performed using a 1:1 binding model and the ForteBio data analysis software. Mean kon, koff values were determined by averaging all binding curves that matched the theoretical fit with an R2 value of ≥0.98.

Binding competition assays: SA biosensors were immersed in KB containing 10µg/ml of biotinylated peptides for 300s, followed by a 20s baseline in KB buffer. Probes were then immersed in KB containing 20µg/ml CV3-25, AMMO1, B6 or CC40.8 for a 300s association phase, followed by a 20s baseline in KB buffer and then immersed into KB containing 20µg/ml CV3-25, AMMO1, B6 or CC40.8 for a 300s association phase.

ELISA

MaxiSorp microtiter plates (Thermo Scientific Cat#464718) were coated with 300ng/well of streptavidin (New England Biolabs Catalog #: N7021S) overnight at room temperature. Plates were washed 4X with PBS with 0.02% Tween-20 (wash buffer), then incubated with 60 µL/well of 3% BSA and 0.02% Tween-20 in PBS (blocking buffer) for 1 hr at 37°C. After washing 4X with wash buffer, 380 ng/well of biotinylated peptides diluted in blocking buffer were incubated for 1 hr at 37°C. Plates were washed 4X in wash buffer and then mAbs were serially diluted in blocking buffer, added to the plate and incubated for 1 hr at 37°C. Plates were washed 4X in wash buffer and the secondary antibody Goat anti-Human Ig-HRP (Southern Biotech, Cat# 2010-05), was added and incubated at 37°C for 1 hr. Plates were washed 4X wash buffer, and then 30µL/well of SureBlue Reserve TMB Peroxidase Substrate (Seracare KPL, Cat# 5120-

0080) was added and incubated for 3 min followed by addition of 30µL of 1 N H2SO4 to stop the reaction. The optical density at 450nm was measured using a SpectraMax i3x plate reader (Molecular Devices). All wash steps were performed using a BioTek 405/TSMicroplate Washer.

Production of CV3-25 Fab

Purified recombinant CV3-25 IgG was mixed with LysC (NEB) at a ratio of 1µg LysC per 10mg of IgG and incubated at 37°C for 18h with nutation. The cleaved product was incubated with 1mL of Protein A resin (GoldBio) per 10mg of initial IgG and incubated at room temp for 1 hr to bind any uncleaved IgG and digested Fc. The purified Fab was further purifed by SEC using a HiLoad 16/600 Superdex 200pg column.

Crystal screening and structure determination

CV3-25 Fab was incubated with 1.5 molar excess of the synthetic stem helix peptide spanning residues 1149-1167 (Genscript). Initial crystal screening was performed by sitting-drop vapor-diffusion in the MCSG Crystallization Suite (Anatrace) using a NT8 drop setter (Formulatrix). Poor diffraction crystals grew in MCSG-3 well B1 and were optimized using the Additive Screen (Hampton Scientific). Diffracting crystals were obtained in a mother liquor (ML) containing 0.1M Na Acetate:HCl, pH 4.5, 2.0M $(NH_4)SO_4$, 0.1M Strontium Chloride. The crystals were cryoprotected by soaking in ML supplemented with 26% glycerol. Diffraction data were collected at Advanced Light Source beamline 5.0.2 at 12286keV. The data set was processed using XDS (Kabsch, 2010) and data reduction was performed using AIMLESS in CCP4 (Winn et al., 2011) to a resolution of 1.74Å. Initial phases were solved by molecular replacement using

Phaser in Phenix (Adams et al., 2010) with a search model of Fab 4AB007 (PDBid: 5MVZ) divided into Fv and Fc portions. Model building was completed using COOT (Emsley and Cowtan, 2004) and refinement was performed in Phenix with the final refinement run through the PDB_REDO server (Joosten et al., 2014). The data collection and refinement statistics are summarized in Supplementary Table 1. Structural figures were made in Pymol (Schrodinger, LLC).

Cell surface SARS-CoV-2 S binding assay.

cDNA corresponding to AA 15-1336 of HCoV-OC43 was PCR amplified from pCAGGS-Flag-HCoV-OC43 Spike (a kind gift from Dr. Marceline Côté, University of Ottawa) and cloned into the pTT3 vector using InFusion cloning (Clontech). A Kozak consensus sequence and the TPA leader sequence (MDAMKRGLCCVLLLCGAVFVSPSAS) was added to the 5' end of the cDNA during PCR amplification. cDNA for the HKU1 spike was PCR amplified from pCMV-HCoV-HKU1 (SinoBiological Cat# VG40606-UT) and subcloned into pTT3.

pTT3-SARS-CoV-2-S (Seydoux et al., 2020), pHDM-MERS-CoV-Spike, pTWist-WIV1-CoV, pHDM-MERS-CoV-1 Spike, pTT3-HKU1 or pTT3-OC43 Spike were transfected into suspension-adapted 293T cells using 293 Free transfection reagent (EMD Millipore Cat# 72181) or PEI transfection reagent (PolySciences Inc. Cat# 23966) according to the manufacturer's instructions. Transfected cells were incubated for 24h at 37ºC with shaking. Meanwhile, 1 µg of each mAb was added to individual wells of a 96 well plate in 50 µl of FACS buffer (PBS + 2% FBS + 1mM EDTA).

Spike-transfected or mock-transfected 293T cells were resuspended at $4x10^6$ cells/ml in FACS buffer and 50µl was added to each well of the 96 well plate. mAb-cell mixture was incubated for 30 minutes on ice. The plates were then washed once with 200µl of FACS buffer and stained with of PE-conjugated AffiniPure Fab fragment goat anti-human IgG (Jackson Immunoresearch Cat# 109-117-008) at a 1:100 dilution and live/dead green fluorescent reactive dye (Thermo Fisher Cat# L34970) at a 1:1000 dilution in 50 µl/well of 1X PBS. The staining reaction was incubated for 20 minutes in the dark on ice. The plates were then washed once with 200µl of FACS buffer and fixed with 50 µl of 10% formalin. The plates were centrifuged, and the formalin was removed and replaced with 250µl of FACS buffer. The % of live PE+ cells was measured on a Guava easyCyte 5HT Flow Cytometer (Luminex). For each mAb, the % of PE+ mock transfected cells was subtracted from the % of PE+ of spike transfected cells.

OC43 live virus neutralization assay.

HCT-8 [HRT-18] cells (ATCC CCL-244™) were seeded at 20,000 cells/well in 96-well plates and cultivated in RPMI containing 10% horse serum and penicillin-streptomycin at 37ºC for 2 days until reaching near confluency. Fifty-fold of the fifty percent tissue culture infection doses ($TCID_{50}$) of OC43 (Zeptometrix Cat#0810024CF) per well was used. Serially diluted serum or mAb was mixed with virus in serum-free RPMI and incubated for 1 h at 33ºC on a shaker at 150 rpm. Then the, virus:antibody mixture was transferred onto HCT-8 cells and the plate was incubated at 33ºC in a CO_2 incubator. At day 5, cells were fixed with -20ºC-cold, 70% MeOH for 15 min. Plate was rinsed with PBS (Gibco) and blocked with PBS containing 2.5 % Blotting grade blocker (Bio-Rad) and 0.05% Tween-20 (Sigma) for 1 hr at 37ºC. After washing one time with PBS-T

(PBS, 0.05% Tween-20), plate was incubated with rabbit anti-nucleocapsid antibody (Sino Biological, Cat# 40643-T62) for 1h at room temperature on a plate shaker at 800 rpm. After that, plate was washed three times with PBS-T and incubated with goat anti-rabbit IgG-HRP (Jackson ImmunoResearch, Cat# 111-035-144) for 1 h at room temperature on a plate shaker at 800 rpm. After washing three times with PBS-T, the assay was developed by addition of 1-Step Ultra TMB-ELISA solution (Thermo Scientific Cat# 34028) and reaction was stopped with 2 N sulfuric acid (Fisher Scientific). Optical density at 450 and 620 nm was captured with SpectraMax M2 (Molecular Devices). Neutralization was defined as the antibody concertation that reduced OD relative to virus control wells (cells + virus only) after subtraction of background OD in cells-only control wells.

NL63 live virus neutralization assay.

LLC-MK2 cells were seeded at 3,000 cells/well in 96-well plate and cultivated in DMEM containing 10% FBS and penicillin-streptomycin at 37ºC for 2 days until reaching near confluency. Fifty-fold of the fifty percent tissue culture infection dose ($TCID_{50}$) of NL63 (BEI resources Cat# NR-470) per well was used. CV3-25 was added to a final concentration of 400 µg/ml and mixed with virus in serum-free RPMI and incubated for 1 h at 33ºC on a shaker at 150 rpm. Wells containing PBS and no virus were included as controls. After the virus and/or virus:antibody mixture was transferred onto LLC-MK2 cells and the plate was incubated at 33ºC in CO_2 incubator. Eight days later the cells were visually inspected for evidence of cytopathic effects under a light microscope.

ACKNOWLEDGEMENTS:

Funding: This work was supported by generous donations to Fred Hutch COVID-19 Research Fund (L.S.), Fast Grants (part of Emergent Ventures at George Mason University) and a COVID pilot award from the Fred Hutch (J.B.) and by the M.J. Murdock Charitable Trust (A.T.M).

X-ray diffraction data was collected at the Berkeley Center for Structural Biology beamline 5.0.2 at the Advanced Light Source (ALS), which is supported in part by the Howard Hughes Medical Institute. ALS is a Department of Energy Office of Science User Facility under Contract No. DE-AC02-05CH11231**.** We thank the James B. Pendleton Charitable Trust for its generous support of Formulatrix robotic instruments. We thank Stephen C. DeRosa and Kristen W Cohen for providing some of the peptides used in this study. **Author Contributions:** Conceptualization, A.T.M., M.P., and L.S.; Investigation, N.K.H., L.J.H., I.S., M.J, A.J.M., Y-H. W., P.Z., J.B. and A.M.H. Writing - Original Draft, N.K.H., A.T.M, M.P. and L.S.; Writing - Review & Editing, All authors.; Funding Acquisition, L.S. and A.T.M. C**ompeting interests:** L.S. and A.T.M. have filed a provisional patent application on the CV3-25 monoclonal antibody. A.T.M. has filed a provisional patent application on the B6 monoclonal antibody. All other authors declare no competing interests. **Data and Materials Availability:** All data are available in the manuscript or the supplementary material. The CV3-25/peptide structure has been deposited in the PDB (7RAQ).

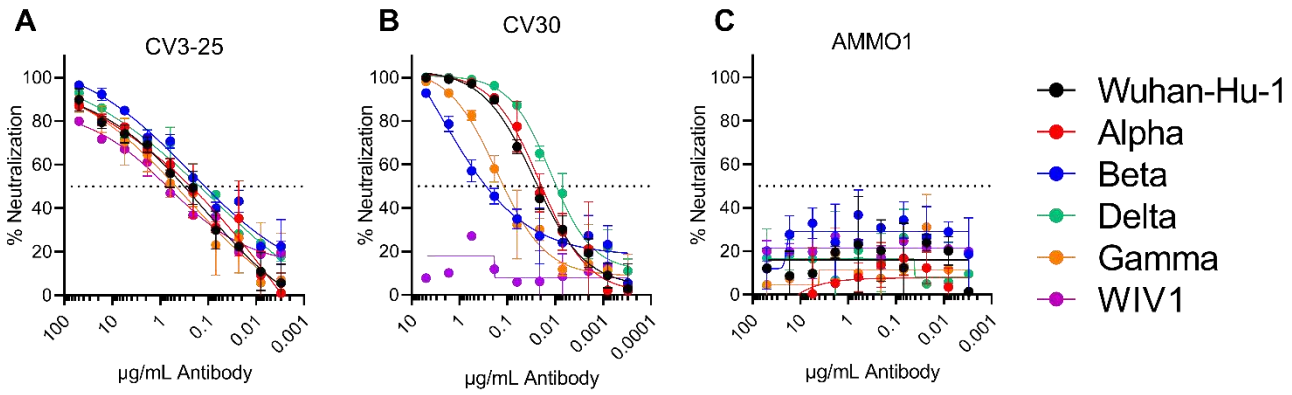

Figure 1. CV3-25 neutralizes SARS-CoV-2 variants and a SARS-like Bat virus. The S2-binding CV3-25 (A), RBD-binding CV30 (B) and anti-EBV mAb AMMO1 (C) were evaluated for their ability to neutralize the indicated SARS-CoV-2 variants of concern and the SARS-like bat virus WIV1.

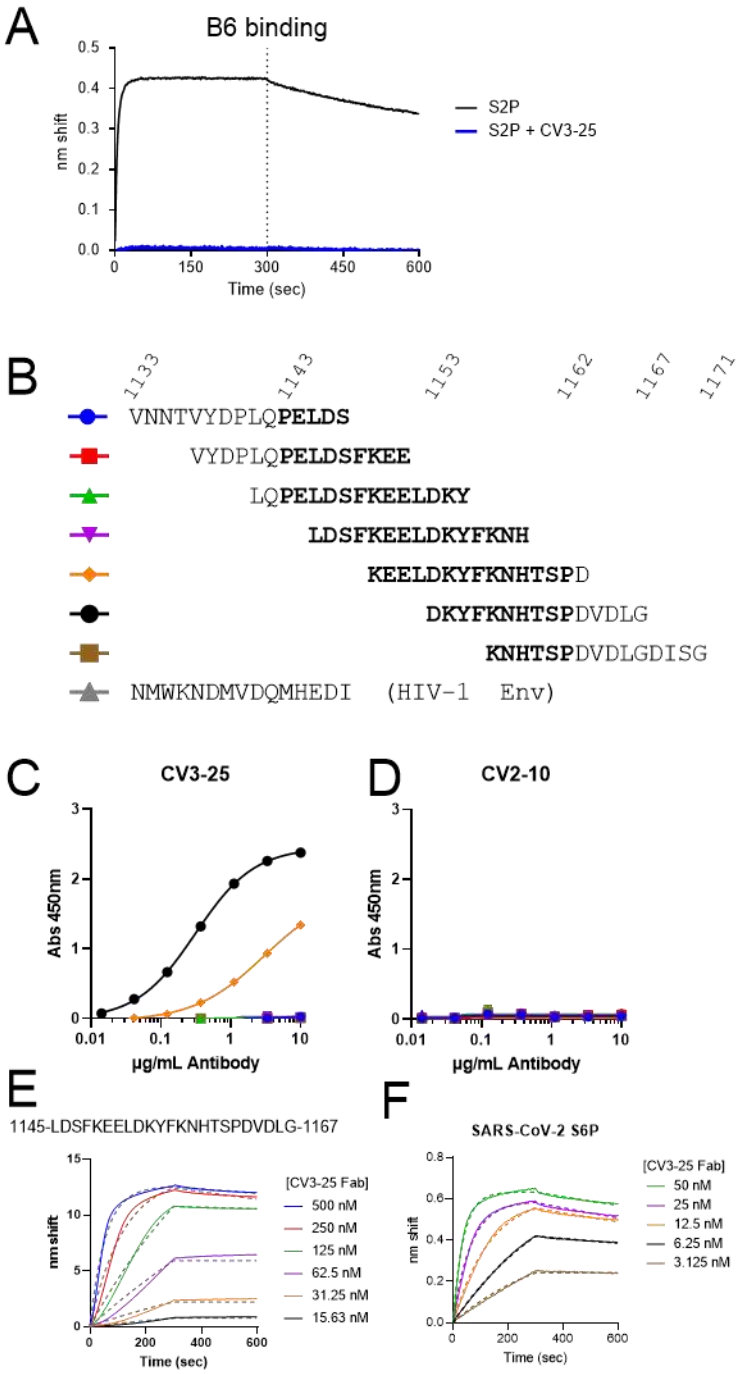

Figure 2. CV3-25 binds to a linear peptide encompassing the C-terminus of the stem helix. (**A**) Binding of the B6 mAb to SARS-CoV-2 S2P alone or a SARS-CoV-2 S2P-CV3-25 complex as indicated. (**B**) Alignment of a set of 15mer peptides that overlap by 11 amino acids spanning residues 1133-1171 of the SARS-CoV-2 spike protein. The region that corresponds to the stem helix in the prefusion wild-type spike protein (based on the 6XR8) is shown in bold. (**C**) CV3-25 was tested for binding to the peptides in **B**, and to a 15mer peptide derived from an HIV-1 Env protein. (**D**) CV2-10, which also binds to S2, but does not compete with CV3-25 was tested for binding to the peptides in **B**. CV3-25 Fab binding was measured to the indicated stem helix peptide (**E**) or a stabilized SARS-CoV-2 spike protein (S6P, **F**) by BLI.

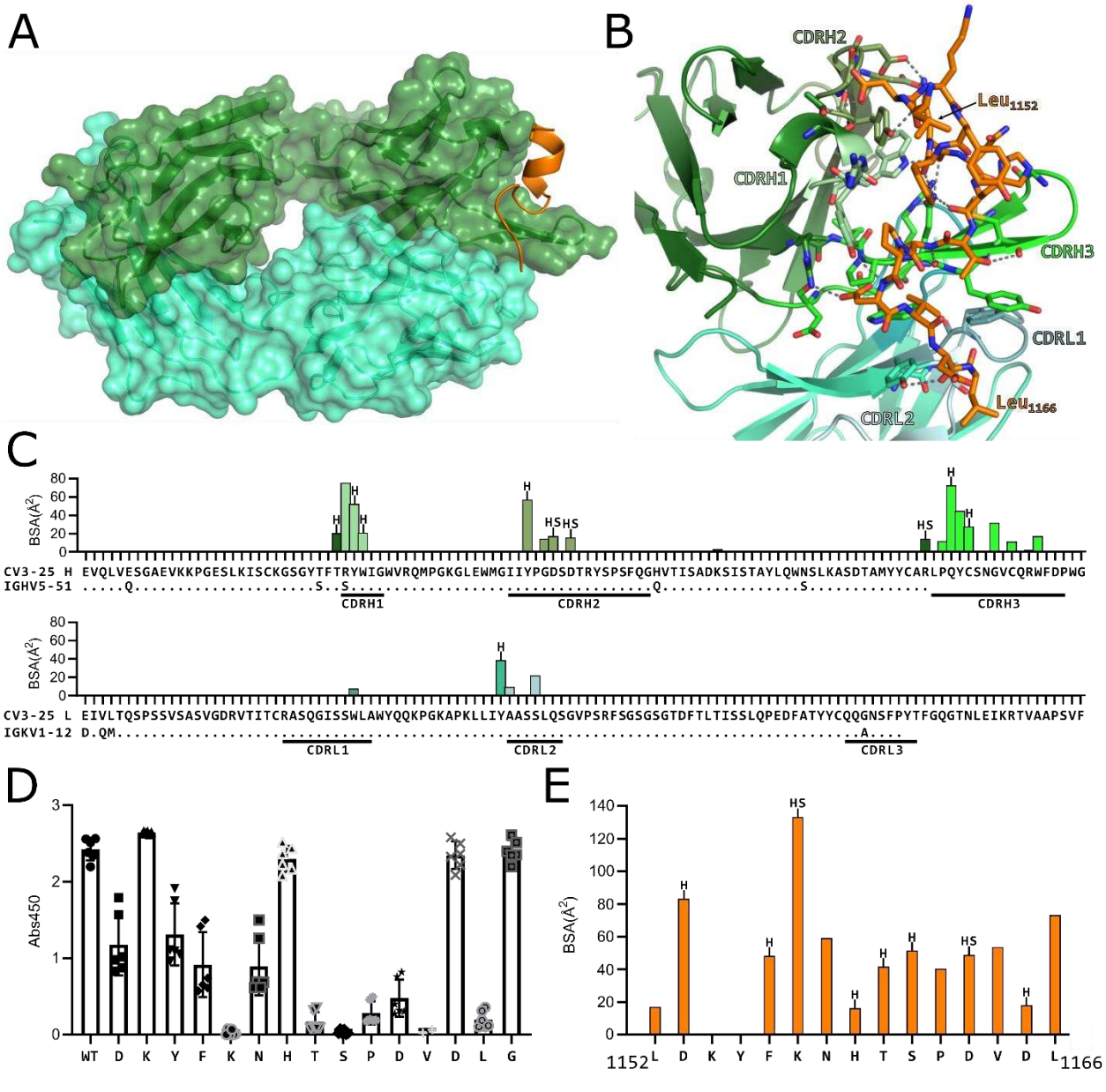

Figure 3. (**A**) **Structure of CV3-25 Fab bound to stem helix peptide.** CV3-25-peptide shown in ribbon structure with mAb surface representation shown in transparency. CV3-25 heavy chain is shown in green and light chain in cyan. The peptide is shown in orange. (**B**) Details of the interactions between the Fab and the peptide. Complementary determining regions (CDRs) are labeled and colored as shown. Hydrogen bonds between Fab residues and the peptide are shown with dashed black

lines. (**C**) Plots of buried surface area (BSA) of each Fab residue interacting with the peptide and a sequence alignment with the corresponding V-gene. CDRs are labelled and color coded to match the structure shown in B. Residues engaged in a hydrogen bond or salt bridge are marked with an “H” or “S”, respectively. (**D**) Alanine scanning plot of the stem helix region that CV3-25 binds. CV3-25 binding to linear peptides corresponding to amino acids 1153-1167 of the SARS-CoV-2 spike, where each amino acid was substituted by alanine was measured by ELISA. The absorbance at 450 nm resulting from the addition of 1.25 µg of CV3-25 is shown. Each dot represents a technical replicate from three independent experiments conducted in duplicate. Full titrations are shown in Figure S1. **(E)** Plot of the BSA of each stem helix peptide residue.

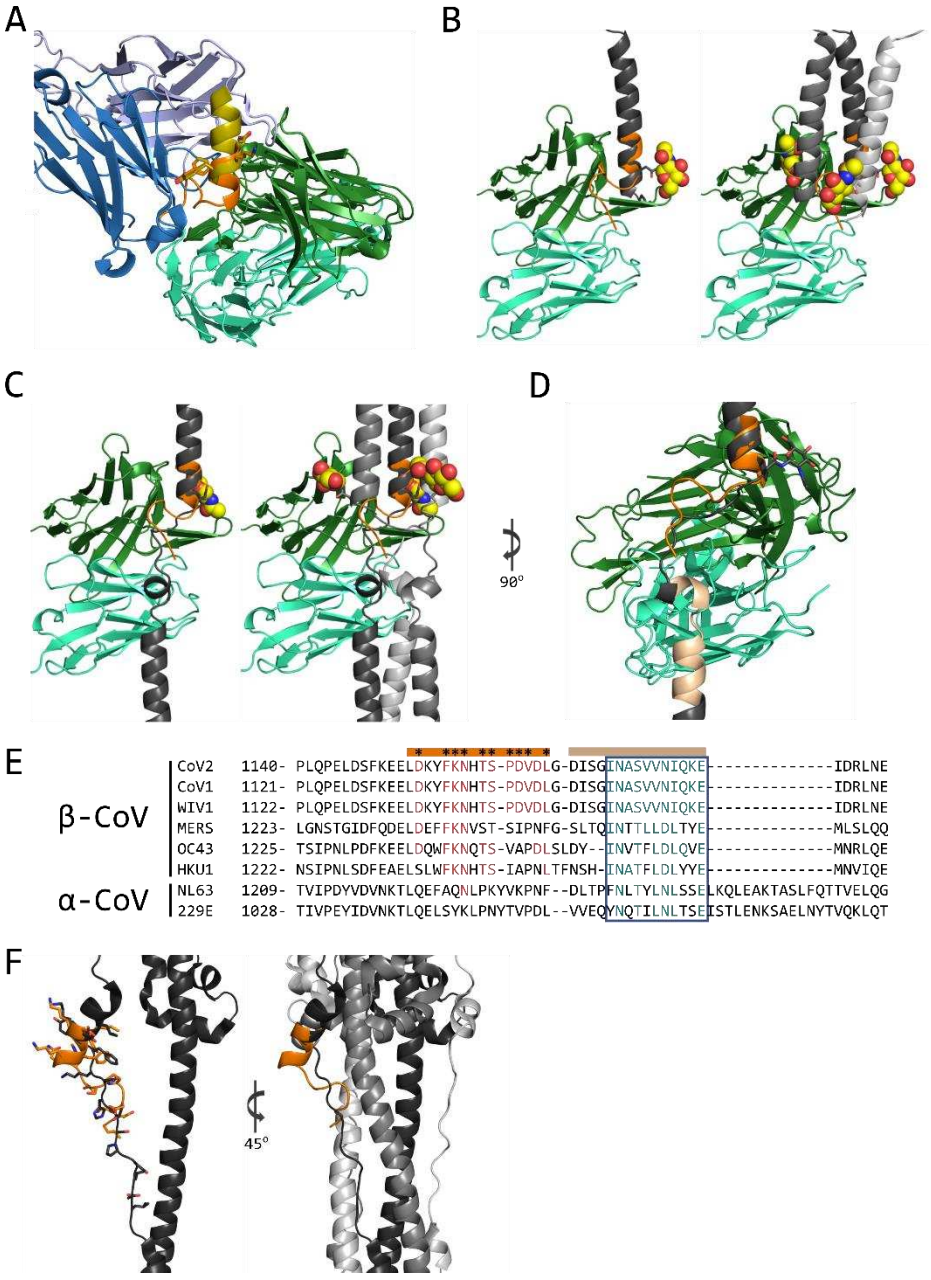

Figure 4. (**A**) Structural alignment of stem helix peptides to CV3-25 Fab and B6 Fab (PDBid: 7M53) shown as ribbon diagram. B6 heavy chain is shown in dark blue and light chain in light blue. CV3-25 heavy chain is shown in green and light chain in cyan. The B6-bound peptide is shown in yellow and the CV3-25-bound peptide in orange. (**B**) Left, structural alignment of the CV3-25 structure and the stem helix structure (PDBid: 6XR8) shown in cartoon representation. The 6XR8 stem helix is shown in dark gray and

682 the CV3-25-bound peptide is shown in orange. Asn_{1158} glycan is shown in yellow sphere
683 representation. Left, the alignment with a single protomer, right, an alignment with the
684 trimer. (**C**) Structural alignment of CV3-25 to MD simulation model of the stem helix and
685 HR2 region of the spike protein (Casalino et al., 2020). Asp_{1158} glycan is shown in
686 yellow sphere representation. Left, an alignment with a single protomer, right an
687 alignment with the trimer. (**D**) Potential interaction area of the N-terminal end of HR2
688 and the light chain of CV3-25 is shown in tan. (**E**) Sequence alignment of the stem helix
689 region of several CoV spike proteins. The peptide bound to CV3-25 is marked by the
690 orange bar and crucial interacting residues are marked by *. The residues conserved in
691 the binding site are shown in red. The region that could interact with the light chain is
692 shown with the tan bar and the conserved region is highlighted by the blue box with
693 similar residues shown in teal. (**F**) Structural alignment of the CV3-25 bound peptide
694 (orange) to the post-fusion S (black, PDBid: 6XRA). The peptide was aligned to
695 $_{1152}$LDKY$_{1155}$ in the spike. Left, the alignment to the protomer. The sidechains of the
696 residues are shown in stick representation, right, the region is shown in context of the
697 trimer.

698

699

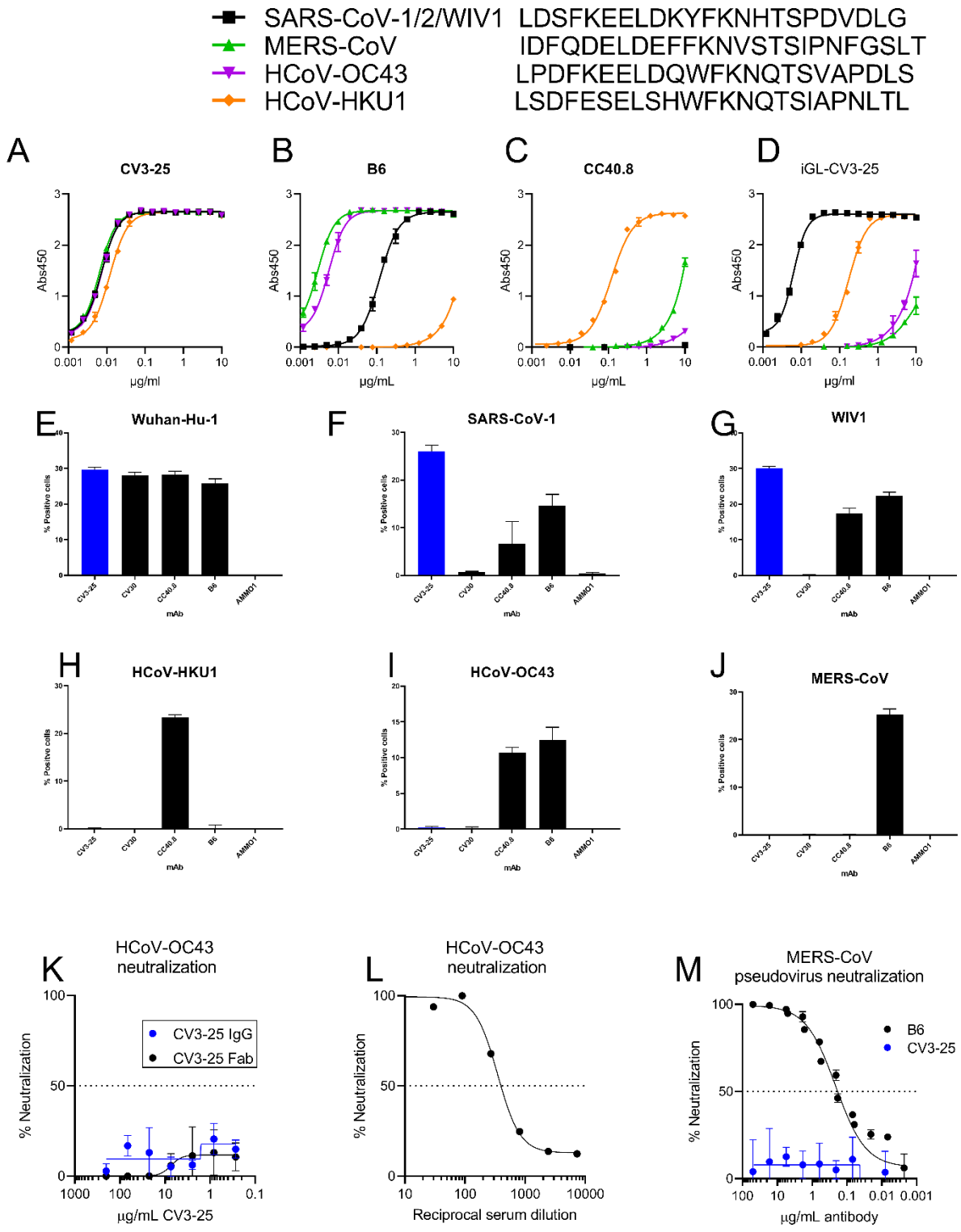

Figure 5. CV3-25 binds to stem helix peptides from diverse betacoronaviruses but only to cell surface-expressed sarbecovirus spike proteins. Binding of CV3-25 (**A**), B6 (**B**), CC40.8 (**C**) or the inferred germline version of CV3-25 (**D**), to linear peptides from SARS-CoV-1/2/WIV1, MERS-CoV, HCoV-OC43, and HCoV-HKU1 was measured by ELISA. Spike proteins from SARS-CoV-2 Wuhan-Hu-1 (**E**), SARS-CoV-1 Urbani (**F**), WIV1 (**G**), HCoV-HKU1 (**H**) and HCoV-OC43 (**I**) and MERS-CoV (**J**) were expressed on the surface of 293 cells, and then stained with the indicated fluorescently labeled mAbs and then analyzed by flow cytometry. The percentage of cells that stained positive with the mAbs is indicated on the y-axis. Neutralization of authentic OC43 by CV3-25 IgG or Fab (**K**), or human sera (**L**). (**M**) Neutralization of MERS-CoV pseudovirus by the indicated mAbs.

References

ADAMS, P. D., AFONINE, P. V., BUNKOCZI, G., CHEN, V. B., DAVIS, I. W., ECHOLS, N., HEADD, J. J., HUNG, L. W., KAPRAL, G. J., GROSSE-KUNSTLEVE, R. W., MCCOY, A. J., MORIARTY, N. W., OEFFNER, R., READ, R. J., RICHARDSON, D. C., RICHARDSON, J. S., TERWILLIGER, T. C. & ZWART, P. H. 2010. PHENIX: a comprehensive Python-based system for macromolecular structure solution. *Acta Crystallogr D Biol Crystallogr,* 66**,** 213-21.

ANDREANO, E., NICASTRI, E., PACIELLO, I., PILERI, P., MANGANARO, N., PICCINI, G., MANENTI, A., PANTANO, E., KABANOVA, A., TROISI, M., VACCA, F., CARDAMONE, D., DE SANTI, C., TORRES, J. L., OZOROWSKI, G., BENINCASA, L., JANG, H., DI GENOVA, C., DEPAU, L., BRUNETTI, J., AGRATI, C., CAPOBIANCHI, M. R., CASTILLETTI, C., EMILIOZZI, A., FABBIANI, M., MONTAGNANI, F., BRACCI, L., SAUTTO, G., ROSS, T. M., MONTOMOLI, E., TEMPERTON, N., WARD, A. B., SALA, C., IPPOLITO, G. & RAPPUOLI, R. 2021. Extremely potent human monoclonal antibodies from COVID-19 convalescent patients. *Cell,* 184**,** 1821-1835.e16.

BROUWER, P. J. M., CANIELS, T. G., VAN DER STRATEN, K., SNITSELAAR, J. L., ALDON, Y., BANGARU, S., TORRES, J. L., OKBA, N. M. A., CLAIREAUX, M., KERSTER, G., BENTLAGE, A. E. H., VAN HAAREN, M. M., GUERRA, D., BURGER, J. A., SCHERMER, E. E., VERHEUL, K. D., VAN DER VELDE, N., VAN DER KOOI, A., VAN SCHOOTEN, J., VAN BREEMEN, M. J., BIJL, T. P. L., SLIEPEN, K., AARTSE, A., DERKING, R., BONTJER, I., KOOTSTRA, N. A., WIERSINGA, W. J., VIDARSSON, G., HAAGMANS, B. L., WARD, A. B., DE BREE, G. J., SANDERS, R. W. & VAN GILS, M. J. 2020. Potent neutralizing antibodies from COVID-19 patients define multiple targets of vulnerability. *Science,* 369**,** 643-650.

CAI, Y., ZHANG, J., XIAO, T., PENG, H., STERLING, S. M., WALSH, R. M., JR., RAWSON, S., RITS-VOLLOCH, S. & CHEN, B. 2020. Distinct conformational states of SARS-CoV-2 spike protein. *Science,* 369**,** 1586-1592.

CAO, Z., LIU, L., DU, L., ZHANG, C., JIANG, S., LI, T. & HE, Y. 2010. Potent and persistent antibody responses against the receptor-binding domain of SARS-CoV spike protein in recovered patients. *Virol J,* 7**,** 299.

CASALINO, L., GAIEB, Z., GOLDSMITH, J. A., HJORTH, C. K., DOMMER, A. C., HARBISON, A. M., FOGARTY, C. A., BARROS, E. P., TAYLOR, B. C., MCLELLAN, J. S., FADDA, E. & AMARO, R. E. 2020. Beyond Shielding: The Roles of Glycans in the SARS-CoV-2 Spike Protein. *ACS Cent Sci,* 6**,** 1722-1734.

CERUTTI, G., GUO, Y., ZHOU, T., GORMAN, J., LEE, M., RAPP, M., REDDEM, E. R., YU, J., BAHNA, F., BIMELA, J., HUANG, Y., KATSAMBA, P. S., LIU, L., NAIR, M. S., RAWI, R., OLIA, A. S., WANG, P., CHUANG, G.-Y., HO, D. D., SHENG, Z., KWONG, P. D. & SHAPIRO, L. 2021. Potent SARS-CoV-2 Neutralizing Antibodies Directed Against Spike N-Terminal Domain Target a Single Supersite. *bioRxiv***,** 2021.01.10.426120.

CHI, X., YAN, R., ZHANG, J., ZHANG, G., ZHANG, Y., HAO, M., ZHANG, Z., FAN, P., DONG, Y., YANG, Y., CHEN, Z., GUO, Y., ZHANG, J., LI, Y., SONG, X., CHEN, Y., XIA, L., FU, L., HOU, L., XU, J., YU, C., LI,

766 J., ZHOU, Q. & CHEN, W. 2020. A neutralizing human antibody binds to the N-terminal domain of
767 the Spike protein of SARS-CoV-2. *Science,* 369**,** 650-655.
768 CLAUSEN, T. M., SANDOVAL, D. R., SPLIID, C. B., PIHL, J., PERRETT, H. R., PAINTER, C. D., NARAYANAN, A.,
769 MAJOWICZ, S. A., KWONG, E. M., MCVICAR, R. N., THACKER, B. E., GLASS, C. A., YANG, Z.,
770 TORRES, J. L., GOLDEN, G. J., BARTELS, P. L., PORELL, R. N., GARRETSON, A. F., LAUBACH, L.,
771 FELDMAN, J., YIN, X., PU, Y., HAUSER, B. M., CARADONNA, T. M., KELLMAN, B. P., MARTINO, C.,
772 GORDTS, P., CHANDA, S. K., SCHMIDT, A. G., GODULA, K., LEIBEL, S. L., JOSE, J., CORBETT, K. D.,
773 WARD, A. B., CARLIN, A. F. & ESKO, J. D. 2020. SARS-CoV-2 Infection Depends on Cellular
774 Heparan Sulfate and ACE2. *Cell,* 183**,** 1043-1057.e15.
775 CRAWFORD, K. H. D., EGUIA, R., DINGENS, A. S., LOES, A. N., MALONE, K. D., WOLF, C. R., CHU, H. Y.,
776 TORTORICI, M. A., VEESLER, D., MURPHY, M., PETTIE, D., KING, N. P., BALAZS, A. B. & BLOOM, J.
777 D. 2020. Protocol and Reagents for Pseudotyping Lentiviral Particles with SARS-CoV-2 Spike
778 Protein for Neutralization Assays. *Viruses,* 12**,** https://doi.org/10.3390/v12050513.
779 CUI, J., LI, F. & SHI, Z. L. 2019. Origin and evolution of pathogenic coronaviruses. *Nat Rev Microbiol,* 17**,**
780 181-192.
781 DONG, E., DU, H. & GARDNER, L. 2020. An interactive web-based dashboard to track COVID-19 in real
782 time. *Lancet Infect Dis,* 20**,** 533-534.
783 EGUIA, R., CRAWFORD, K. H. D., STEVENS-AYERS, T., KELNHOFER-MILLEVOLTE, L., GRENINGER, A. L.,
784 ENGLUND, J. A., BOECKH, M. J. & BLOOM, J. D. 2020. A human coronavirus evolves antigenically
785 to escape antibody immunity. *bioRxiv***,** 2020.12.17.423313.
786 EMSLEY, P. & COWTAN, K. 2004. Coot: model-building tools for molecular graphics. *Acta Crystallogr D*
787 *Biol Crystallogr,* 60**,** 2126-32.
788 ESPOSITO, D., MEHALKO, J., DREW, M., SNEAD, K., WALL, V., TAYLOR, T., FRANK, P., DENSON, J. P.,
789 HONG, M., GULTEN, G., SADTLER, K., MESSING, S. & GILLETTE, W. 2020. Optimizing high-yield
790 production of SARS-CoV-2 soluble spike trimers for serology assays. *Protein Expr Purif,* 174**,**
791 105686.
792 FARIA, N. R., CLARO, I. M., CANDIDO, D., FRANCO, L. A. M., ANDRADE, P. S., COLETTI, T. M., SILVA, C. A.
793 M., SALES, F. C., MANULI, E. R., AGUIAR, R. S., GABURO, N., CAMILO, C. D. C., FRAIJI, N. A.,
794 CRISPIM, M. A. E., CARVALHO, M. D. P. S. S., RAMBAUT, A., LOMAN, N., PYBUS, O. G., SABINO, E.
795 C. & NETWORK, C. G. 2021. Genomic characterisation of an emergent SARS-CoV-2 lineage in
796 Manaus: preliminary findings. *Virological.org***,** https://virological.org/t/genomic-
797 characterisation-of-an-emergent-sars-cov-2-lineage-in-manaus-preliminary-findings/586.
798 GE, X. Y., LI, J. L., YANG, X. L., CHMURA, A. A., ZHU, G., EPSTEIN, J. H., MAZET, J. K., HU, B., ZHANG, W.,
799 PENG, C., ZHANG, Y. J., LUO, C. M., TAN, B., WANG, N., ZHU, Y., CRAMERI, G., ZHANG, S. Y.,
800 WANG, L. F., DASZAK, P. & SHI, Z. L. 2013. Isolation and characterization of a bat SARS-like
801 coronavirus that uses the ACE2 receptor. *Nature,* 503**,** 535-8.
802 GHAI, R. R., CARPENTER, A., LIEW, A. Y., MARTIN, K. B., HERRING, M. K., GERBER, S. I., HALL, A. J.,
803 SLEEMAN, J. M., VONDOBSCHUETZ, S. & BEHRAVESH, C. B. 2021. Animal Reservoirs and Hosts
804 for Emerging Alphacoronaviruses and Betacoronaviruses. *Emerg Infect Dis,* 27**,** 1015-1022.
805 GUI, M., SONG, W., ZHOU, H., XU, J., CHEN, S., XIANG, Y. & WANG, X. 2017. Cryo-electron microscopy
806 structures of the SARS-CoV spike glycoprotein reveal a prerequisite conformational state for
807 receptor binding. *Cell Res,* 27**,** 119-129.
808 HOFFMANN, M., KLEINE-WEBER, H., SCHROEDER, S., KRUGER, N., HERRLER, T., ERICHSEN, S.,
809 SCHIERGENS, T. S., HERRLER, G., WU, N. H., NITSCHE, A., MULLER, M. A., DROSTEN, C. &
810 POHLMANN, S. 2020. SARS-CoV-2 Cell Entry Depends on ACE2 and TMPRSS2 and Is Blocked by a
811 Clinically Proven Protease Inhibitor. *Cell,* 181**,** 271-280.e8.

812 HOFMANN, H., PYRC, K., VAN DER HOEK, L., GEIER, M., BERKHOUT, B. & PÖHLMANN, S. 2005. Human
813 coronavirus NL63 employs the severe acute respiratory syndrome coronavirus receptor for
814 cellular entry. *Proc Natl Acad Sci U S A,* 102**,** 7988-93.
815 HUANG, Y., NGUYEN, A. W., HSIEH, C.-L., SILVA, R., OLALUWOYE, O. S., WILEN, R. E., KAOUD, T. S.,
816 AZOUZ, L. R., QERQEZ, A. N., LE, K. C., BOHANON, A. L., DIVENERE, A. M., LIU, Y., LEE, A. G.,
817 AMENGOR, D., DALBY, K. N., D'ARCY, S., MCLELLAN, J. S. & MAYNARD, J. A. 2021. Identification
818 of a conserved neutralizing epitope present on spike proteins from all highly pathogenic
819 coronaviruses. *bioRxiv***,** 2021.01.31.428824.
820 HURLBURT, N. K., SEYDOUX, E., WAN, Y. H., EDARA, V. V., STUART, A. B., FENG, J., SUTHAR, M. S.,
821 MCGUIRE, A. T., STAMATATOS, L. & PANCERA, M. 2020. Structural basis for potent
822 neutralization of SARS-CoV-2 and role of antibody affinity maturation. *Nat Commun,* 11**,** 5413.
823 HWANG, W. C., LIN, Y., SANTELLI, E., SUI, J., JAROSZEWSKI, L., STEC, B., FARZAN, M., MARASCO, W. A. &
824 LIDDINGTON, R. C. 2006. Structural basis of neutralization by a human anti-severe acute
825 respiratory syndrome spike protein antibody, 80R. *J Biol Chem,* 281**,** 34610-6.
826 JENNEWEIN, M. F., MACCAMY, A. J., AKINS, N. R., FENG, J., HOMAD, L. J., HURLBURT, N. K., SEYDOUX, E.,
827 WAN, Y.-H., STUART, A. B., EDARA, V. V., FLOYD, K., VANDERHEIDEN, A., MASCOLA, J. R., DORIA-
828 ROSE, N., WANG, L., YANG, E. S., CHU, H. Y., TORRES, J. L., OZOROWSKI, G., WARD, A. B.,
829 WHALEY, R. E., COHEN, K. W., PANCERA, M., MCELRATH, M. J., ENGLUND, J. A., FINZI, A.,
830 SUTHAR, M. S., MCGUIRE, A. T. & STAMATATOS, L. 2021. Isolation and Characterization of Cross-
831 Neutralizing Coronavirus Antibodies from COVID-19+ Subjects. *Cell Reports,* 36**,** 109353.
832 JIANG, L., WANG, N., ZUO, T., SHI, X., POON, K. M., WU, Y., GAO, F., LI, D., WANG, R., GUO, J., FU, L.,
833 YUEN, K. Y., ZHENG, B. J., WANG, X. & ZHANG, L. 2014. Potent neutralization of MERS-CoV by
834 human neutralizing monoclonal antibodies to the viral spike glycoprotein. *Sci Transl Med,* 6**,**
835 234ra59.
836 JOOSTEN, R. P., LONG, F., MURSHUDOV, G. N. & PERRAKIS, A. 2014. The PDB_REDO server for
837 macromolecular structure model optimization. *IUCrJ,* 1**,** 213-20.
838 KABSCH, W. 2010. XDS. *Acta Crystallogr D Biol Crystallogr,* 66**,** 125-32.
839 KE, Z., OTON, J., QU, K., CORTESE, M., ZILA, V., MCKEANE, L., NAKANE, T., ZIVANOV, J., NEUFELDT, C. J.,
840 CERIKAN, B., LU, J. M., PEUKES, J., XIONG, X., KRÄUSSLICH, H. G., SCHERES, S. H. W.,
841 BARTENSCHLAGER, R. & BRIGGS, J. A. G. 2020. Structures and distributions of SARS-CoV-2 spike
842 proteins on intact virions. *Nature,* 588**,** 498-502.
843 KHOURY, D. S., CROMER, D., REYNALDI, A., SCHLUB, T. E., WHEATLEY, A. K., JUNO, J. A., SUBBARAO, K.,
844 KENT, S. J., TRICCAS, J. A. & DAVENPORT, M. P. 2021. Neutralizing antibody levels are highly
845 predictive of immune protection from symptomatic SARS-CoV-2 infection. *Nat Med*.
846 KIRCHDOERFER, R. N., WANG, N., PALLESEN, J., WRAPP, D., TURNER, H. L., COTTRELL, C. A., CORBETT, K.
847 S., GRAHAM, B. S., MCLELLAN, J. S. & WARD, A. B. 2018. Stabilized coronavirus spikes are
848 resistant to conformational changes induced by receptor recognition or proteolysis. *Sci Rep,* 8**,**
849 15701.
850 KISTLER, K. E. & BEDFORD, T. 2021. Evidence for adaptive evolution in the receptor-binding domain of
851 seasonal coronaviruses OC43 and 229E. *Elife,* 10**,** e64509.
852 LI, W., MOORE, M. J., VASILIEVA, N., SUI, J., WONG, S. K., BERNE, M. A., SOMASUNDARAN, M.,
853 SULLIVAN, J. L., LUZURIAGA, K., GREENOUGH, T. C., CHOE, H. & FARZAN, M. 2003. Angiotensin-
854 converting enzyme 2 is a functional receptor for the SARS coronavirus. *Nature,* 426**,** 450-4.
855 LIU, L., WANG, P., NAIR, M. S., YU, J., RAPP, M., WANG, Q., LUO, Y., CHAN, J. F., SAHI, V., FIGUEROA, A.,
856 GUO, X. V., CERUTTI, G., BIMELA, J., GORMAN, J., ZHOU, T., CHEN, Z., YUEN, K. Y., KWONG, P. D.,
857 SODROSKI, J. G., YIN, M. T., SHENG, Z., HUANG, Y., SHAPIRO, L. & HO, D. D. 2020. Potent
858 neutralizing antibodies against multiple epitopes on SARS-CoV-2 spike. *Nature,* 584**,** 450-456.

LUMLEY, S. F., O'DONNELL, D., STOESSER, N. E., MATTHEWS, P. C., HOWARTH, A., HATCH, S. B., MARSDEN, B. D., COX, S., JAMES, T., WARREN, F., PECK, L. J., RITTER, T. G., DE TOLEDO, Z., WARREN, L., AXTEN, D., CORNALL, R. J., JONES, E. Y., STUART, D. I., SCREATON, G., EBNER, D., HOOSDALLY, S., CHAND, M., CROOK, D. W., O'DONNELL, A. M., CONLON, C. P., POUWELS, K. B., WALKER, A. S., PETO, T. E. A., HOPKINS, S., WALKER, T. M., JEFFERY, K., EYRE, D. W. & OXFORD UNIVERSITY HOSPITALS STAFF TESTING, G. 2021. Antibody Status and Incidence of SARS-CoV-2 Infection in Health Care Workers. *N Engl J Med,* 384**,** 533-540.

MCCALLUM, M., MARCO, A. D., LEMPP, F., TORTORICI, M. A., PINTO, D., WALLS, A. C., BELTRAMELLO, M., CHEN, A., LIU, Z., ZATTA, F., ZEPEDA, S., DI IULIO, J., BOWEN, J. E., MONTIEL-RUIZ, M., ZHOU, J., ROSEN, L. E., BIANCHI, S., GUARINO, B., FREGNI, C. S., ABDELNABI, R., CAROLINE FOO, S.-Y., ROTHLAUF, P. W., BLOYET, L.-M., BENIGNI, F., CAMERONI, E., NEYTS, J., RIVA, A., SNELL, G., TELENTI, A., WHELAN, S. P. J., VIRGIN, H. W., CORTI, D., PIZZUTO, M. S. & VEESLER, D. 2021. N-terminal domain antigenic mapping reveals a site of vulnerability for SARS-CoV-2. *bioRxiv***,** 2021.01.14.426475.

MCMAHAN, K., YU, J., MERCADO, N. B., LOOS, C., TOSTANOSKI, L. H., CHANDRASHEKAR, A., LIU, J., PETER, L., ATYEO, C., ZHU, A., BONDZIE, E. A., DAGOTTO, G., GEBRE, M. S., JACOB-DOLAN, C., LI, Z., NAMPANYA, F., PATEL, S., PESSAINT, L., VAN RY, A., BLADE, K., YALLEY-OGUNRO, J., CABUS, M., BROWN, R., COOK, A., TEOW, E., ANDERSEN, H., LEWIS, M. G., LAUFFENBURGER, D. A., ALTER, G. & BAROUCH, D. H. 2020. Correlates of protection against SARS-CoV-2 in rhesus macaques. *Nature,* 590**,** 630-634.

MILLET, J. K. & WHITTAKER, G. R. 2015. Host cell proteases: Critical determinants of coronavirus tropism and pathogenesis. *Virus Res,* 202**,** 120-34.

NIU, P., ZHANG, S., ZHOU, P., HUANG, B., DENG, Y., QIN, K., WANG, P., WANG, W., WANG, X., ZHOU, J., ZHANG, L. & TAN, W. 2018. Ultrapotent Human Neutralizing Antibody Repertoires Against Middle East Respiratory Syndrome Coronavirus From a Recovered Patient. *J Infect Dis,* 218**,** 1249-1260.

PALLESEN, J., WANG, N., CORBETT, K. S., WRAPP, D., KIRCHDOERFER, R. N., TURNER, H. L., COTTRELL, C. A., BECKER, M. M., WANG, L., SHI, W., KONG, W. P., ANDRES, E. L., KETTENBACH, A. N., DENISON, M. R., CHAPPELL, J. D., GRAHAM, B. S., WARD, A. B. & MCLELLAN, J. S. 2017. Immunogenicity and structures of a rationally designed prefusion MERS-CoV spike antigen. *Proc Natl Acad Sci U S A,* 114**,** E7348-E7357.

PICCOLI, L., PARK, Y. J., TORTORICI, M. A., CZUDNOCHOWSKI, N., WALLS, A. C., BELTRAMELLO, M., SILACCI-FREGNI, C., PINTO, D., ROSEN, L. E., BOWEN, J. E., ACTON, O. J., JACONI, S., GUARINO, B., MINOLA, A., ZATTA, F., SPRUGASCI, N., BASSI, J., PETER, A., DE MARCO, A., NIX, J. C., MELE, F., JOVIC, S., RODRIGUEZ, B. F., GUPTA, S. V., JIN, F., PIUMATTI, G., LO PRESTI, G., PELLANDA, A. F., BIGGIOGERO, M., TARKOWSKI, M., PIZZUTO, M. S., CAMERONI, E., HAVENAR-DAUGHTON, C., SMITHEY, M., HONG, D., LEPORI, V., ALBANESE, E., CESCHI, A., BERNASCONI, E., ELZI, L., FERRARI, P., GARZONI, C., RIVA, A., SNELL, G., SALLUSTO, F., FINK, K., VIRGIN, H. W., LANZAVECCHIA, A., CORTI, D. & VEESLER, D. 2020. Mapping Neutralizing and Immunodominant Sites on the SARS-CoV-2 Spike Receptor-Binding Domain by Structure-Guided High-Resolution Serology. *Cell,* 183**,** 1024-1042.e21.

PINTO, D., SAUER, M. M., CZUDNOCHOWSKI, N., LOW, J. S., TORTORICI, M. A., HOUSLEY, M. P., NOACK, J., WALLS, A. C., BOWEN, J. E., GUARINO, B., ROSEN, L. E., DI IULIO, J., JERAK, J., KAISER, H., ISLAM, S., JACONI, S., SPRUGASCI, N., CULAP, K., ABDELNABI, R., FOO, C., COELMONT, L., BARTHA, I., BIANCHI, S., SILACCI-FREGNI, C., BASSI, J., MARZI, R., VETTI, E., CASSOTTA, A., CESCHI, A., FERRARI, P., CIPPÀ, P. E., GIANNINI, O., CERUTI, S., GARZONI, C., RIVA, A., BENIGNI, F., CAMERONI, E., PICCOLI, L., PIZZUTO, M. S., SMITHEY, M., HONG, D., TELENTI, A., LEMPP, F. A., NEYTS, J., HAVENAR-DAUGHTON, C., LANZAVECCHIA, A., SALLUSTO, F., SNELL, G., VIRGIN, H. W.,

BELTRAMELLO, M., CORTI, D. & VEESLER, D. 2021. A human antibody that broadly neutralizes betacoronaviruses protects against SARS-CoV-2 by blocking the fusion machinery. *bioRxiv*, 2021.05.09.442808.

PRABAKARAN, P., GAN, J., FENG, Y., ZHU, Z., CHOUDHRY, V., XIAO, X., JI, X. & DIMITROV, D. S. 2006. Structure of severe acute respiratory syndrome coronavirus receptor-binding domain complexed with neutralizing antibody. *J Biol Chem,* 281**,** 15829-36.

RAMBAUT, A., LOMAN, N., PYBUS, O., BARCLAY, W., BARRETT, J., CARABELLI, A., CONNOR, T., PEACOCK, T., ROBERTSON, D. L. & VOLZ, E. 2020. *Preliminary genomic characterisation of an emergent SARS-CoV-2 lineage in the UK defined by a novel set of spike mutations* [Online]. virological.org. Available: https://virological.org/t/preliminary-genomic-characterisation-of-an-emergent-sars-cov-2-lineage-in-the-uk-defined-by-a-novel-set-of-spike-mutations/563 [Accessed January 18, 2021 2021].

ROCKX, B., CORTI, D., DONALDSON, E., SHEAHAN, T., STADLER, K., LANZAVECCHIA, A. & BARIC, R. 2008. Structural basis for potent cross-neutralizing human monoclonal antibody protection against lethal human and zoonotic severe acute respiratory syndrome coronavirus challenge. *J Virol,* 82**,** 3220-35.

ROGERS, T. F., ZHAO, F., HUANG, D., BEUTLER, N., BURNS, A., HE, W. T., LIMBO, O., SMITH, C., SONG, G., WOEHL, J., YANG, L., ABBOTT, R. K., CALLAGHAN, S., GARCIA, E., HURTADO, J., PARREN, M., PENG, L., RAMIREZ, S., RICKETTS, J., RICCIARDI, M. J., RAWLINGS, S. A., WU, N. C., YUAN, M., SMITH, D. M., NEMAZEE, D., TEIJARO, J. R., VOSS, J. E., WILSON, I. A., ANDRABI, R., BRINEY, B., LANDAIS, E., SOK, D., JARDINE, J. G. & BURTON, D. R. 2020. Isolation of potent SARS-CoV-2 neutralizing antibodies and protection from disease in a small animal model. *Science,* 369**,** 956-963.

SAKHARKAR, M., RAPPAZZO, C. G., WIELAND-ALTER, W. F., HSIEH, C. L., WRAPP, D., ESTERMAN, E. S., KAKU, C. I., WEC, A. Z., GEOGHEGAN, J. C., MCLELLAN, J. S., CONNOR, R. I., WRIGHT, P. F. & WALKER, L. M. 2021. Prolonged evolution of the human B cell response to SARS-CoV-2 infection. *Sci Immunol,* 6.

SAUER, M. M., TORTORICI, M. A., PARK, Y. J., WALLS, A. C., HOMAD, L., ACTON, O. J., BOWEN, J. E., WANG, C., XIONG, X., DE VAN DER SCHUEREN, W., QUISPE, J., HOFFSTROM, B. G., BOSCH, B. J., MCGUIRE, A. T. & VEESLER, D. 2021. Structural basis for broad coronavirus neutralization. *Nat Struct Mol Biol,* 28**,** 478-486.

SEYDOUX, E., HOMAD, L. J., MACCAMY, A. J., PARKS, K. R., HURLBURT, N. K., JENNEWEIN, M. F., AKINS, N. R., STUART, A. B., WAN, Y. H., FENG, J., WHALEY, R. E., SINGH, S., BOECKH, M., COHEN, K. W., MCELRATH, M. J., ENGLUND, J. A., CHU, H. Y., PANCERA, M., MCGUIRE, A. T. & STAMATATOS, L. 2020. Analysis of a SARS-CoV-2-Infected Individual Reveals Development of Potent Neutralizing Antibodies with Limited Somatic Mutation. *Immunity,* 53**,** 98-105 e5.

SHAH, P., CANZIANI, G. A., CARTER, E. P. & CHAIKEN, I. 2021. The Case for S2: The Potential Benefits of the S2 Subunit of the SARS-CoV-2 Spike Protein as an Immunogen in Fighting the COVID-19 Pandemic. *Front Immunol,* 12**,** 637651.

SNIJDER, J., ORTEGO, M. S., WEIDLE, C., STUART, A. B., GRAY, M. D., MCELRATH, M. J., PANCERA, M., VEESLER, D. & MCGUIRE, A. T. 2018. An Antibody Targeting the Fusion Machinery Neutralizes Dual-Tropic Infection and Defines a Site of Vulnerability on Epstein-Barr Virus. *Immunity,* 48**,** 799-811 e9.

SONG, G., HE, W. T., CALLAGHAN, S., ANZANELLO, F., HUANG, D., RICKETTS, J., TORRES, J. L., BEUTLER, N., PENG, L., VARGAS, S., CASSELL, J., PARREN, M., YANG, L., IGNACIO, C., SMITH, D. M., VOSS, J. E., NEMAZEE, D., WARD, A. B., ROGERS, T., BURTON, D. R. & ANDRABI, R. 2020. Cross-reactive serum and memory B cell responses to spike protein in SARS-CoV-2 and endemic coronavirus infection. *bioRxiv*, 2020.09.22.308965.

STAMATATOS, L., CZARTOSKI, J., WAN, Y. H., HOMAD, L. J., RUBIN, V., GLANTZ, H., NERADILEK, M., SEYDOUX, E., JENNEWEIN, M. F., MACCAMY, A. J., FENG, J., MIZE, G., DE ROSA, S. C., FINZI, A., LEMOS, M. P., COHEN, K. W., MOODIE, Z., MCELRATH, M. J. & MCGUIRE, A. T. 2021. mRNA vaccination boosts cross-variant neutralizing antibodies elicited by SARS-CoV-2 infection. *Science*.

SUI, J., LI, W., MURAKAMI, A., TAMIN, A., MATTHEWS, L. J., WONG, S. K., MOORE, M. J., TALLARICO, A. S., OLURINDE, M., CHOE, H., ANDERSON, L. J., BELLINI, W. J., FARZAN, M. & MARASCO, W. A. 2004. Potent neutralization of severe acute respiratory syndrome (SARS) coronavirus by a human mAb to S1 protein that blocks receptor association. *Proc Natl Acad Sci U S A,* 101**,** 2536-41.

TANG, X. C., AGNIHOTHRAM, S. S., JIAO, Y., STANHOPE, J., GRAHAM, R. L., PETERSON, E. C., AVNIR, Y., TALLARICO, A. S., SHEEHAN, J., ZHU, Q., BARIC, R. S. & MARASCO, W. A. 2014. Identification of human neutralizing antibodies against MERS-CoV and their role in virus adaptive evolution. *Proc Natl Acad Sci U S A,* 111**,** E2018-26.

TEGALLY, H., WILKINSON, E., GIOVANETTI, M., IRANZADEH, A., FONSECA, V., GIANDHARI, J., DOOLABH, D., PILLAY, S., SAN, E. J., MSOMI, N., MLISANA, K., VON GOTTBERG, A., WALAZA, S., ALLAM, M., ISMAIL, A., MOHALE, T., GLASS, A. J., ENGELBRECHT, S., VAN ZYL, G., PREISER, W., PETRUCCIONE, F., SIGAL, A., HARDIE, D., MARAIS, G., HSIAO, M., KORSMAN, S., DAVIES, M.-A., TYERS, L., MUDAU, I., YORK, D., MASLO, C., GOEDHALS, D., ABRAHAMS, S., LAGUDA-AKINGBA, O., ALISOLTANI-DEHKORDI, A., GODZIK, A., WIBMER, C. K., SEWELL, B. T., LOURENÇO, J., ALCANTARA, L. C. J., POND, S. L. K., WEAVER, S., MARTIN, D., LESSELLS, R. J., BHIMAN, J. N., WILLIAMSON, C. & DE OLIVEIRA, T. 2020. Emergence and rapid spread of a new severe acute respiratory syndrome-related coronavirus 2 (SARS-CoV-2) lineage with multiple spike mutations in South Africa. *medRxiv***,** 2020.12.21.20248640.

TORTORICI, M. A. & VEESLER, D. 2019. Structural insights into coronavirus entry. *Adv Virus Res,* 105**,** 93-116.

TRAGGIAI, E., BECKER, S., SUBBARAO, K., KOLESNIKOVA, L., UEMATSU, Y., GISMONDO, M. R., MURPHY, B. R., RAPPUOLI, R. & LANZAVECCHIA, A. 2004. An efficient method to make human monoclonal antibodies from memory B cells: potent neutralization of SARS coronavirus. *Nat Med,* 10**,** 871-5.

TURONOVA, B., SIKORA, M., SCHURMANN, C., HAGEN, W. J. H., WELSCH, S., BLANC, F. E. C., VON BULOW, S., GECHT, M., BAGOLA, K., HORNER, C., VAN ZANDBERGEN, G., LANDRY, J., DE AZEVEDO, N. T. D., MOSALAGANTI, S., SCHWARZ, A., COVINO, R., MUHLEBACH, M. D., HUMMER, G., KRIJNSE LOCKER, J. & BECK, M. 2020. In situ structural analysis of SARS-CoV-2 spike reveals flexibility mediated by three hinges. *Science,* 370**,** 203-208.

ULLAH, I., PRÉVOST, J., LADINSKY, M. S., STONE, H., LU, M., ANAND, S. P., BEAUDOIN-BUSSIÈRES, G., SYMMES, K., BENLARBI, M., DING, S., GASSER, R., FINK, C., CHEN, Y., TAUZIN, A., GOYETTE, G., BOURASSA, C., MEDJAHED, H., MACK, M., CHUNG, K., WILEN, C. B., DEKABAN, G. A., DIKEAKOS, J. D., BRUCE, E. A., KAUFMANN, D. E., STAMATATOS, L., MCGUIRE, A. T., RICHARD, J., PAZGIER, M., BJORKMAN, P. J., MOTHES, W., FINZI, A., KUMAR, P. & UCHIL, P. D. 2021. Live Imaging of SARS-CoV-2 Infection in Mice Reveals Neutralizing Antibodies Require Fc Function for Optimal Efficacy. *bioRxiv***,** 2021.03.22.436337.

VLASAK, R., LUYTJES, W., SPAAN, W. & PALESE, P. 1988. Human and bovine coronaviruses recognize sialic acid-containing receptors similar to those of influenza C viruses. *Proc Natl Acad Sci U S A,* 85**,** 4526-9.

WALLS, A. C., PARK, Y. J., TORTORICI, M. A., WALL, A., MCGUIRE, A. T. & VEESLER, D. 2020. Structure, Function, and Antigenicity of the SARS-CoV-2 Spike Glycoprotein. *Cell,* 181**,** 281-292.e6.

WALLS, A. C., XIONG, X., PARK, Y. J., TORTORICI, M. A., SNIJDER, J., QUISPE, J., CAMERONI, E., GOPAL, R., DAI, M., LANZAVECCHIA, A., ZAMBON, M., REY, F. A., CORTI, D. & VEESLER, D. 2019. Unexpected

Receptor Functional Mimicry Elucidates Activation of Coronavirus Fusion. *Cell,* 176**,** 1026-1039.e15.

WAN, Y., SHANG, J., GRAHAM, R., BARIC, R. S. & LI, F. 2020. Receptor Recognition by the Novel Coronavirus from Wuhan: an Analysis Based on Decade-Long Structural Studies of SARS Coronavirus. *J Virol,* 94**,** e00127-20.

WANG, C., VAN HAPEREN, R., GUTIÉRREZ-ÁLVAREZ, J., LI, W., OKBA, N. M. A., ALBULESCU, I., WIDJAJA, I., VAN DIEREN, B., FERNANDEZ-DELGADO, R., SOLA, I., HURDISS, D. L., DARAMOLA, O., GROSVELD, F., VAN KUPPEVELD, F. J. M., HAAGMANS, B. L., ENJUANES, L., DRABEK, D. & BOSCH, B.-J. 2020. Isolation of cross-reactive monoclonal antibodies against divergent human coronaviruses that delineate a conserved and vulnerable site on the spike protein. *bioRxiv***,** 2020.10.20.346916.

WANG, C., VAN HAPEREN, R., GUTIÉRREZ-ÁLVAREZ, J., LI, W., OKBA, N. M. A., ALBULESCU, I., WIDJAJA, I., VAN DIEREN, B., FERNANDEZ-DELGADO, R., SOLA, I., HURDISS, D. L., DARAMOLA, O., GROSVELD, F., VAN KUPPEVELD, F. J. M., HAAGMANS, B. L., ENJUANES, L., DRABEK, D. & BOSCH, B. J. 2021. A conserved immunogenic and vulnerable site on the coronavirus spike protein delineated by cross-reactive monoclonal antibodies. *Nat Commun,* 12**,** 1715.

WEINREICH, D. M., SIVAPALASINGAM, S., NORTON, T., ALI, S., GAO, H., BHORE, R., MUSSER, B. J., SOO, Y., ROFAIL, D., IM, J., PERRY, C., PAN, C., HOSAIN, R., MAHMOOD, A., DAVIS, J. D., TURNER, K. C., HOOPER, A. T., HAMILTON, J. D., BAUM, A., KYRATSOUS, C. A., KIM, Y., COOK, A., KAMPMAN, W., KOHLI, A., SACHDEVA, Y., GRABER, X., KOWAL, B., DICIOCCIO, T., STAHL, N., LIPSICH, L., BRAUNSTEIN, N., HERMAN, G. & YANCOPOULOS, G. D. 2021. REGN-COV2, a Neutralizing Antibody Cocktail, in Outpatients with Covid-19. *N Engl J Med,* 384**,** 238-251.

WILLIAMS, C. J., HEADD, J. J., MORIARTY, N. W., PRISANT, M. G., VIDEAU, L. L., DEIS, L. N., VERMA, V., KEEDY, D. A., HINTZE, B. J., CHEN, V. B., JAIN, S., LEWIS, S. M., ARENDALL, W. B., 3RD, SNOEYINK, J., ADAMS, P. D., LOVELL, S. C., RICHARDSON, J. S. & RICHARDSON, D. C. 2018. MolProbity: More and better reference data for improved all-atom structure validation. *Protein Sci,* 27**,** 293-315.

WINN, M. D., BALLARD, C. C., COWTAN, K. D., DODSON, E. J., EMSLEY, P., EVANS, P. R., KEEGAN, R. M., KRISSINEL, E. B., LESLIE, A. G., MCCOY, A., MCNICHOLAS, S. J., MURSHUDOV, G. N., PANNU, N. S., POTTERTON, E. A., POWELL, H. R., READ, R. J., VAGIN, A. & WILSON, K. S. 2011. Overview of the CCP4 suite and current developments. *Acta Crystallogr D Biol Crystallogr,* 67**,** 235-42.

WOO, P. C., LAU, S. K., HUANG, Y. & YUEN, K. Y. 2009. Coronavirus diversity, phylogeny and interspecies jumping. *Exp Biol Med (Maywood),* 234**,** 1117-27.

WRAPP, D., WANG, N., CORBETT, K. S., GOLDSMITH, J. A., HSIEH, C. L., ABIONA, O., GRAHAM, B. S. & MCLELLAN, J. S. 2020. Cryo-EM structure of the 2019-nCoV spike in the prefusion conformation. *Science,* 367**,** 1260-1263.

YEAGER, C. L., ASHMUN, R. A., WILLIAMS, R. K., CARDELLICHIO, C. B., SHAPIRO, L. H., LOOK, A. T. & HOLMES, K. V. 1992. Human aminopeptidase N is a receptor for human coronavirus 229E. *Nature,* 357**,** 420-2.

YING, T., DU, L., JU, T. W., PRABAKARAN, P., LAU, C. C., LU, L., LIU, Q., WANG, L., FENG, Y., WANG, Y., ZHENG, B. J., YUEN, K. Y., JIANG, S. & DIMITROV, D. S. 2014. Exceptionally potent neutralization of Middle East respiratory syndrome coronavirus by human monoclonal antibodies. *J Virol,* 88**,** 7796-805.

YUAN, Y., CAO, D., ZHANG, Y., MA, J., QI, J., WANG, Q., LU, G., WU, Y., YAN, J., SHI, Y., ZHANG, X. & GAO, G. F. 2017. Cryo-EM structures of MERS-CoV and SARS-CoV spike glycoproteins reveal the dynamic receptor binding domains. *Nat Commun,* 8**,** 15092.

ZHOU, P., YUAN, M., SONG, G., BEUTLER, N., SHAABANI, N., HUANG, D., HE, W.-T., ZHU, X., CALLAGHAN, S., YONG, P., ANZANELLO, F., PENG, L., RICKETTS, J., PARREN, M., GARCIA, E., RAWLINGS, S. A., SMITH, D. M., NEMAZEE, D., TEIJARO, J. R., ROGERS, T. F., WILSON, I. A., BURTON, D. R. &

ANDRABI, R. 2021. A protective broadly cross-reactive human antibody defines a conserved site of vulnerability on beta-coronavirus spikes. *bioRxiv*, 2021.03.30.437769.

Supplemental Information

Supplementary Table 1. Data collection and refinement statistics for crystal structure

	CV3-25 Fab + Spike peptide 1149-1167
Data collection	
Space group	$P3_221$
Cell dimensions	
a, *b*, *c* (Å)	60.173, 60.173, 285.825
α, *β*, *γ* (°)	90, 90, 120
Resolution (Å)	49.01-1.740 (1.77-1.74)
R_{merge}[a]	0.025 (0.309)
<I/σ(I)>	21.7 (2.7)
$CC_{1/2}$	0.999 (0.670)
Completeness	100 (100)
Redundancy	1.9 (1.9)
Refinement	
Resolution (Å)	48.96-1.74 (2.18-1.74)
No. unique reflections	63190 (6196)
R_{work}[b]/R_{free}[c]	18.64/20.90 (34.85/35.03)
No. atoms	3825
Protein	3479
Water	294
Ligand	52
B-factors (Å^2)	36.1
Protein	35.24
Water	42.33
Ligand	58.63
RMS bond length (Å)	0.012
RMS bond angle (°)	1.57
Ramachadran Plot Statistics[d]	
Residues	455
Most Favored region	97.54
Allowed Region	2.46
Disallowed Region	0.00
Clashscore	1.43
PDB ID	**7RAQ**

[a] $R_{merge} = [\sum_h\sum_i|I_h - I_{hi}|/\sum_h\sum_i I_{hi}]$ where I_h is the mean of I_{hi} observations of reflection *h*. Numbers in parenthesis represent highest resolution shell. [b] R_{factor} and [c] $R_{free} = \sum||F_{obs}| - |F_{calc}|| / \sum|F_{obs}| \times 100$ for 95% of recorded data (R_{factor}) or 5% data (R_{free}). [c] MolProbity (Williams et al., 2018)

1060

1061 Table S2 CV3-25 binding kinetics

	K_D (M)X10^{-9}	k_{on} (1/Ms)X105	K_{on} error (1/Ms)X10^{3}	K_{off} (1/s)X10^{-4}	K_{off} error (1/s)X10^{-5}
SARS-CoV-2 stem helix peptide	5.23	0.3	5.8	1.59	1.24
SARS-CoV-2 S6P	0.66	6.0	4.23	3.89	0.72

1062

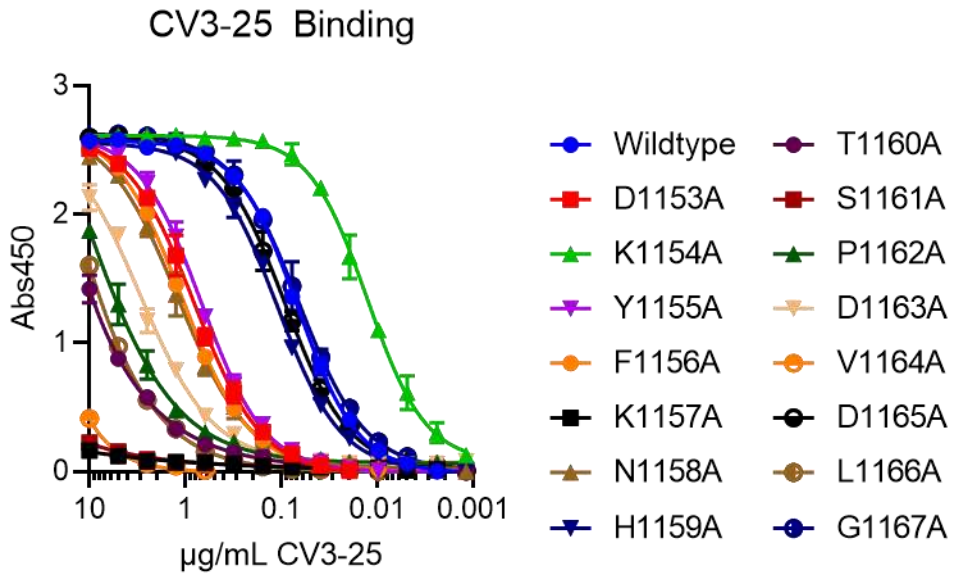

1063

1064

1065 **Figure S1.** CV3-25 binding to linear peptides corresponding to amino acids 1153-1167
1066 of the SARS-CoV-2 spike, where each amino acid was substituted to alanine, was
1067 measured by ELISA.

1068

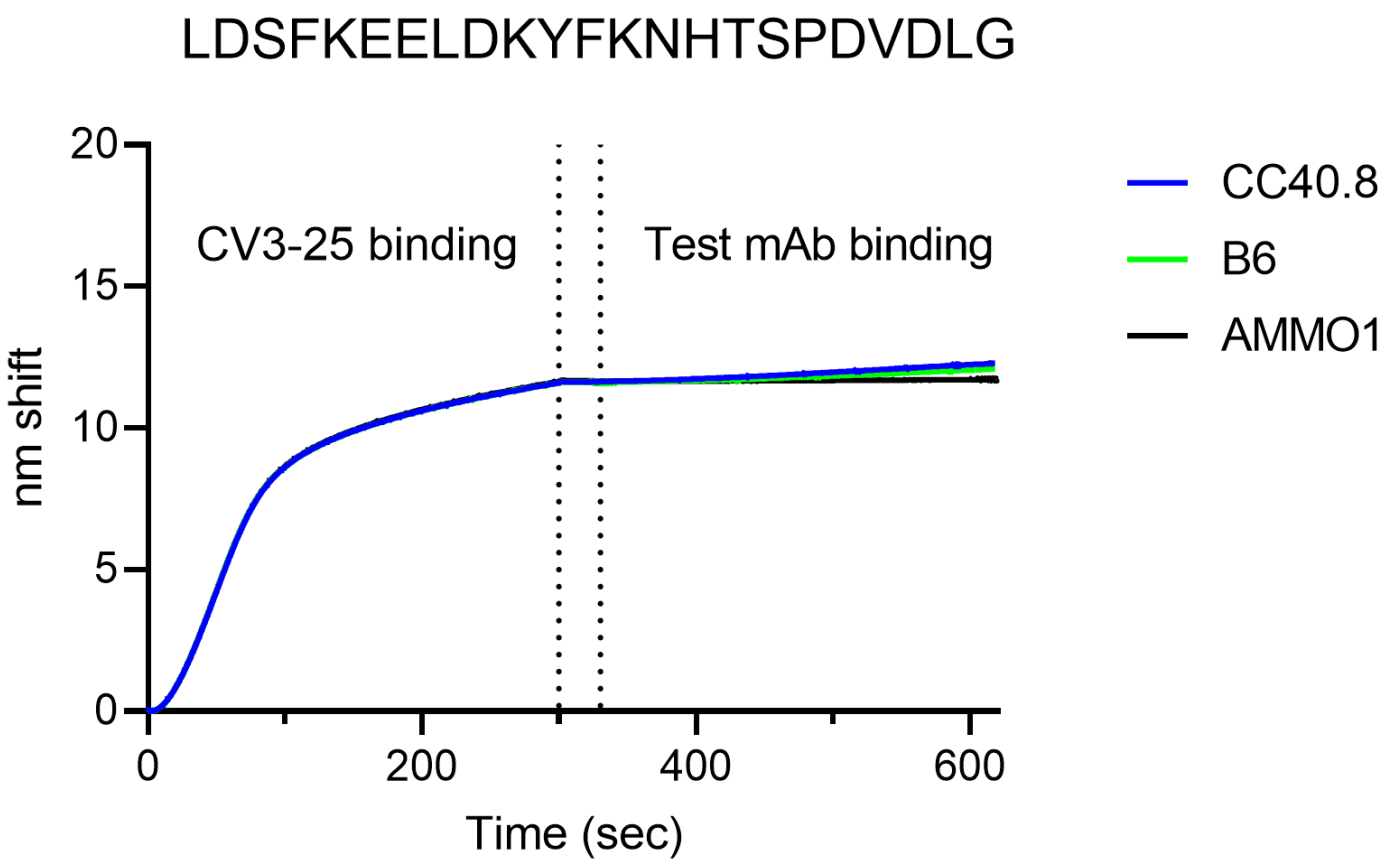

Fig.S2 CV3-25 competes with stem-helix directed neutralizing mAbs. The indicated SARS-CoV-2 peptide was immobilized on a streptavidin biosensor and immersed into a solution containing CV3-25 for 300s. The sensor was then immersed in kinetics buffer for 30 seconds and then immersed in kinetics buffer containing B6, CC40.8 or AMMO1 as indicated. The dotted lines demarcate the initial binding, baseline, and second binding steps.

1077

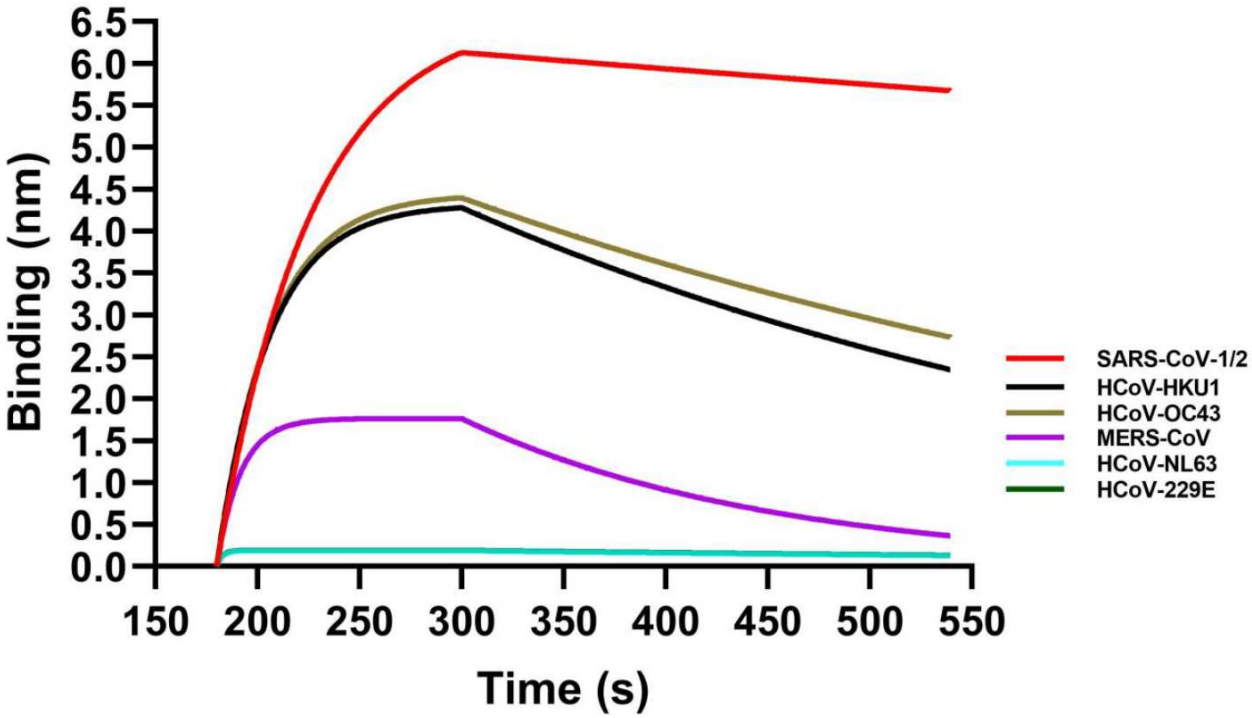

1078 **Figure S3:** CV3-25 binds to linear peptides from diverse Beta CoVs as measured by
1079 BLI. Binding of CV3-25 to linear stem helix-derived peptides from the indicated CoVs
1080 (Zhou et al., 2021) was measured by BLI.

1081

1082

1083

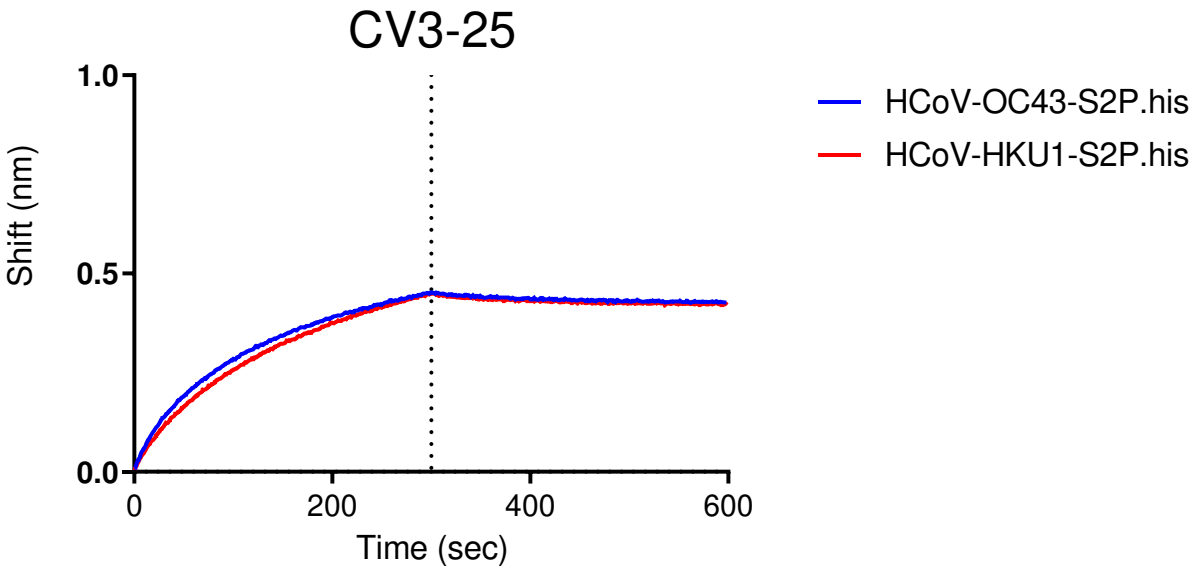

1084 **Figure S4:** CV3-25 binds to stabilized spike ectodomains from HCoV-OC43 and HCoV-
1085 HKU1 as measured by BLI as indicated.

1086

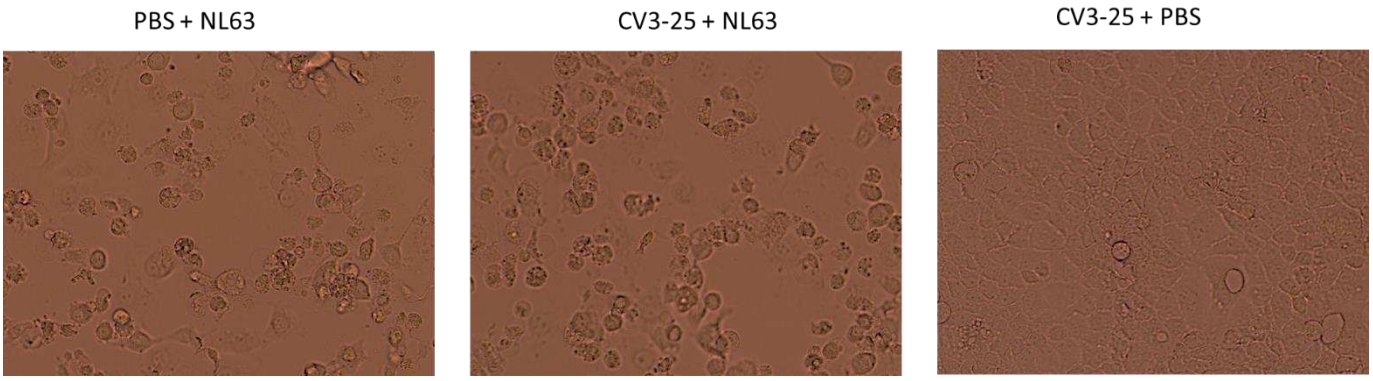

Figure S5. CV3-25 does not neutralize HCoV-NL63. LLC-MK2 cells were incubated with 50X $TCID_{50}$ NL63 with PBS or 50X $TCID_{50}$ NL63 plus 400 µg/ml CV3-25, or with 400 µg/ml CV3-25 in PBS as indicated. 8 days later the cells were examined for cytopathic effects on a light microscope. Representative images from one of four wells for each condition are shown.